



Cenozoic volcanism and extension in northwestern Mesa Central, Durango, México

Isidro Loza-Aguirre^{1,2,*}, Ángel F. Nieto-Samaniego¹, Susana A. Alaniz-Álvarez¹, Carlos Ortega-Obregón¹

¹Centro de Geociencias, Universidad Nacional Autónoma de México, Campus Juriquilla, Boulevard Juriquilla No. 3001, Juriquilla, Querétaro, México, CP 76230.

²Centro de Geociencias, Posgrado en Ciencias de la Tierra, Universidad Nacional Autónoma de México, Campus Juriquilla, Boulevard Juriquilla No. 3001, Juriquilla, Querétaro, México, CP 76230.

*isla@geociencias.unam.mx

Abstract

The Santiago Papasquiaro region is located in the northwest portion of the Mesa Central and is characterized by Tertiary Sierra Madre Occidental lithology. Geologic mapping and dating of key units using U-Pb laser ablation method on zircons has identified three different lithostratigraphic groups. These include: (1) early Eocene felsic volcanic rocks, consisting of the Antigua ignimbrite [51.75 +0.35/-0.45 Ma]; (2) late Eocene - early Oligocene felsic to intermediate volcanic rocks, consisting of the Altamira ignimbrite [38.8 ± 1.0 Ma], El Cazadero andesite [ages of 37.2 +0.30/-0.40 Ma and 35.95 +0.45/-0.5 Ma], a dioritic intrusion, the Venadita rhyolite, Puente Negro ignimbrite [34.0 +0.50/-0.70 Ma], Los Fresnos ignimbrite and Balín ignimbrite [33.2 +0.50/-0.20 Ma]; and (3) late Oligocene to Quaternary sedimentary and volcanic mafic rocks comprising the Santiago sedimentary formation, basalts equivalent to Metates Formation and Neogene to Quaternary continental non-consolidated deposits. Within the studied area, the main volcanic pulse of the Sierra Madre Occidental volcanic province corresponds to the second group, which lasted *ca.* 5 Ma. Older rocks are represented by a single outcrop of the Antigua ignimbrite, and the younger units are mainly continental clastic sediments intercalated with sporadic mafic alkaline volcanic rocks that record a major change in the tectonic regime. Extension that began in late Eocene - Oligocene gradually tilted the late Eocene – early Oligocene volcanic sequence and formed the NNW-trending Santiago Papasquiaro half-graben, which is the northernmost and earliest structure of the Río Chico-Otinapa graben. NW-striking faults of the San Luis-Tepehuanes fault system were synchronous with the development of the Santiago Papasquiaro half-graben. The deformation propagated gradually to the south, forming the NNW Río Chico-Otinapa graben by the early-middle Miocene, and to the east-southeast in the Santiaguillo graben. A recent minor extensional deformation accommodated by NE-striking faults was probably related to seismic deformation of the Nuevo Ideal zone, approximately 40 km southeast of the study area.

Keywords: Cenozoic, stratigraphy, extension, Mesa Central, Sierra Madre Occidental, graben system.

Resumen

La región de Santiago Papasquiaro está localizada en el noroeste de la Mesa Central y está caracterizada por litología terciaria de la Sierra Madre Occidental. Mediante la cartografía geológica del área y la realización de fechamientos isotópicos por el método U-Pb de ablación láser en circones se reconocieron tres grupos litoestratigráficos. Estos incluyen: (1) rocas volcánicas félasicas del Eoceno temprano, que consiste de la ignimbrita Antigua [51.75 +0.35/-0.45 Ma]; (2) rocas volcánicas félasicas a intermedias del Eoceno tardío-Oligoceno temprano, que incluye a la ignimbrita Altamira [38.7 ± 1.0 Ma], la andesita El Cazadero [edades de 37.2 +0.30/-0.40 Ma y 35.95 +0.45/-0.5 Ma], una intrusión diorítica, la riolita Venadita, la ignimbrita Puente Negro [34.0 +0.50/-0.70 Ma], la ignimbrita Los Fresnos y la ignimbrita Balín [33.2 +0.50/-0.20 Ma]; y (3) rocas sedimentarias continentales y volcánicas

máficas del Oligoceno tardío-Cuaternario que comprenden a la formación Santiago, basaltos equivalentes a la Formación Metates y sedimentos continentales no consolidados del Neógeno-Cuaternario. En la zona de estudio el pulso volcánico más importante de la provincia volcánica de la Sierra Madre Occidental corresponde al segundo grupo, que duró ca. 5 Ma. Las rocas más antiguas están representadas por un afloramiento de la ignimbrita Antigua, y las unidades más jóvenes son principalmente sedimentos clásticos continentales intercalados con esporádicas rocas volcánicas máficas alcalinas, que registran un cambio importante en el régimen tectónico. La extensión que comenzó en el Eoceno tardío-Oligoceno basculó gradualmente a la secuencia volcánica del Eoceno tardío-Oligoceno temprano y formó al semigraben de Santiago Papasquiaro de rumbo NNW, que es la estructura más septentrional, y primera en desarrollarse del graben de Río Chico-Otinapa. La actividad en las fallas de rumbo NW del Sistema de fallas San Luis-Tepehuanes fue sincrónica con el desarrollo del semigraben de Santiago Papasquiaro. La deformación se propagó gradualmente hacia el Sur, desarrollándose el graben de Río Chico-Otinapa de rumbo NNW durante el Mioceno temprano-medio, y hacia el Este-Sureste en el graben de Santiaguillo. La deformación menor extensional reciente acomodada por fallas de rumbo NE, estuvo relacionada probablemente con la actividad sísmica en la zona de Nuevo Ideal, 40 km al sureste del área de estudio.

Palabras clave: Cenozoico, Estratigrafía, Extensión, Mesa Central, Sierra Madre Occidental, sistema de graben.

1. Introduction

Santiago Papasquiaro is located in central Mexico in the northwestern portion of the Mesa Central physiographic province (MC) (Nieto-Samaniego *et al.*, 2005), almost 130 km northwest from Durango City (Figure 1 A, B). The most recent geological studies in the zone are the Santiago Papasquiaro geological maps published by the Servicio Geológico Mexicano at scales of 1:250000 (Mungía-Rojas *et al.*, 2000) and 1:50000 (Luévan-Pinedo *et al.*, 2003), as well as the study of Nieto-Samaniego *et al.* (2012) about the stratigraphy, deformation and seismicity in the Santiaguillo graben, located 40 km southeast of Santiago Papasquiaro (Figure 1 C). This region is characterized by outcrops of Tertiary volcanic rocks of the Sierra Madre Occidental volcanic province (SMOc) (Ferrari *et al.*, 2005) (Figure 1C and 2).

Regional structures in the study area strike from NE to NW (Mungía-Rojas *et al.*, 2000; Luévan-Pinedo *et al.*, 2003; Nieto-Samaniego *et al.*, 2005). NE faults are poorly known, although in some regions of the SMOc they act as transfer zones between domains of different tilts (Henry and Aranda-Gómez, 2000). NNE to NNW-striking grabens are located within the Sierra Madre Occidental (SMOc) and the Mesa Central (MC), one of the most noticeable of these structures is the ~150 km long Río Chico-Otinapa graben (RCOG) (Figures 1 and 3) (Aranda-Gómez *et al.*, 1997; Henry and Aranda-Gómez, 2000). In previous studies the NW faults have been considered part of the San Luis-Tepehuanes Fault System (SLTFS) (Nieto-Samaniego *et al.*, 2005, 2012). The SLTFS is a major structure that crosses central Mexico from San Luis de La Paz, Gto., to Tepehuanes, Dgo., consisting of normal faults that had been active from Eocene to Quaternary time (Figure 1 C). In the NW segment, southeast of Santiago Papasquiaro, the SLTFS had associated Quaternary magmatism and seismic activity (Figures 1 C and 2) (Nieto-Samaniego *et al.*, 2005, 2012). Part of the northwestern segment of the SLTFS intersects

the northernmost portion of the RCOG within the study area (Figures 1 and 3).

Representative volcanic units of the study area were dated with U-Pb on zircons using a spot of 23 microns of laser ablation attached to an inductively coupled plasma mass spectrometer (LA-ICP-MS). All of these ages were obtained at the Laboratorio de Estudio Isotópicos (LEI), Centro de Geociencias, UNAM. Detailed methodology of this technique and data reduction procedures used in this laboratory are described by Solari *et al.* (2010) and Solari and Tanner (2011). Due to the lack of common lead (^{204}Pb) values (*e.g.*, from feldspars) of these rocks, we use the algebraic method of correction of Andersen (2002) with a careful analysis on Tera-Wasserburg concordia diagrams. Analyses that show evidence of inclusions or lead loss were discarded during data reduction procedure and only the most concordant ages were used to determine the mean age using the Zircon Age Extractor script from Ludwig (2008).

The knowledge of the Tertiary lithostratigraphy and volcanic activity pulses, as well as the relative ages of major structures and their relationship with volcanism, in the Santiago Papasquiaro region is certainly poor compared with other areas of the MC as Guanajuato, San Luis Potosí and Zacatecas (Nieto-Samaniego *et al.*, 2005). The geologic mapping carried out on the 1:50000 scale G13C48 Santiago Papasquiaro topographic base map (INEGI, 2000), allows inferring the relationships among deformation, volcanic activity and major structures during Cenozoic time in this area, which are the main objectives of this work. Based on the geologic mapping and the new isotopic ages reported in this contribution, an improved lithostratigraphic column and a reconstruction of the main volcanic and faulting events are proposed.

2. Geological setting

In this portion of the MC the lithological record

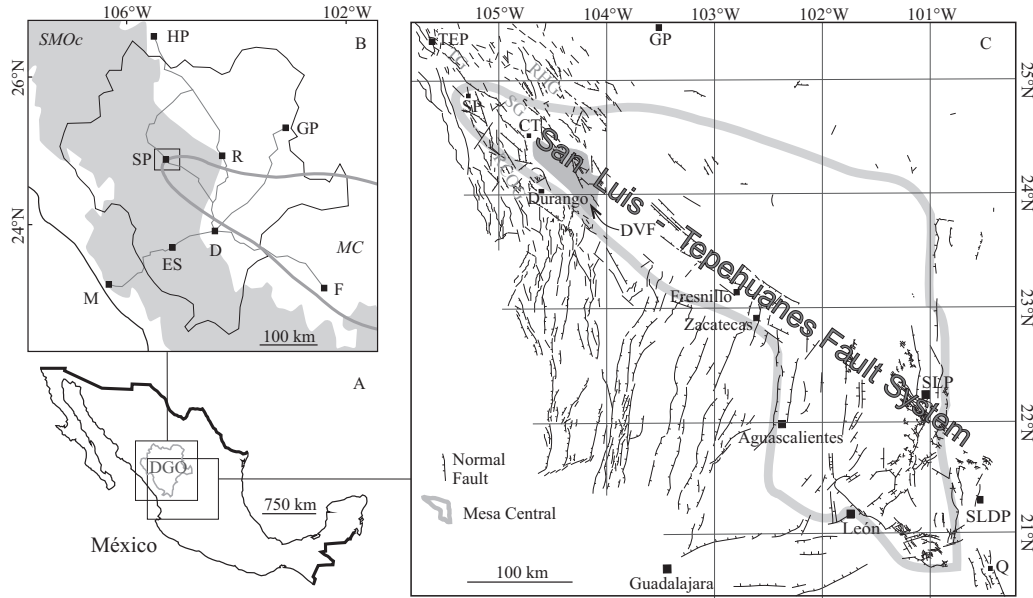


Figure 1. Geographic location of the study area. A) Durango State is located in central northwest México. B) Light gray thin lines represent the roads that connect the principal cities and towns in the region: Hidalgo del Parral (HP), Gómez Palacio (GP), Rodeo (R), Santiago Papasquiaro (SP), Mazatlán (M), El Salto (ES); Fresnillo (F), Durango (D). Gray shaded area represents the Sierra Madre Occidental volcanic province (SMOc) (Ferrari *et al.*, 2005), and the Mesa Central (MC) is delimited by thick gray line (Nieto-Samaniego *et al.*, 2005). The box enclosing SP represents the study area. C) Regional structural map of the Mesa Central and surroundings (Modified from Nieto-Samaniego *et al.*, 2005). The San Luis – Tepehuanes Fault System has a NW general strike and a length of almost 600 km from San Luis de La Paz in the southeast (SLDP) to Tepehuanes in the northwest (TEP). In the northwest in gray text: Tepehuanes Graben (TG), Rodeo Half Graben (RHG), Santiaguillo Graben (SG) and Río Chico-Otinapa Graben (RCOG). Durango Quaternary Volcanic Field (DVF) is northeast of Durango City. San Luis Potosí City (SLP), Querétaro City (Q). The Mesa Central is delimited by thick gray line.

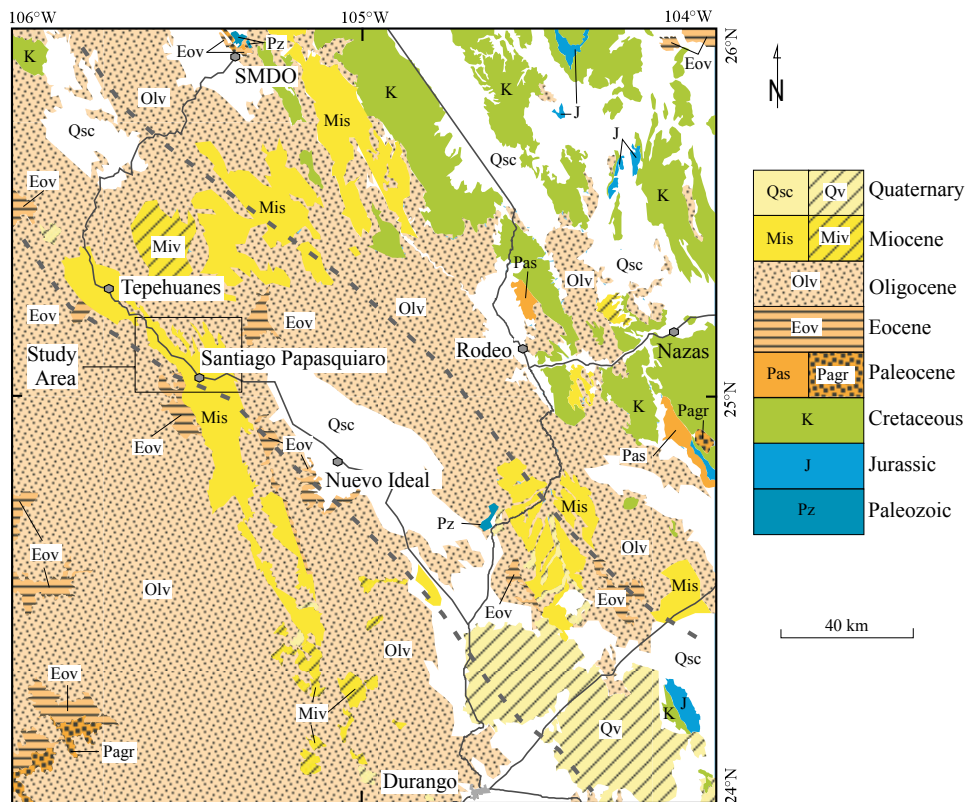


Figure 2. Regional geological map of the northwestern Mesa Central in the region between Durango and Santa María del Oro (SMDO). Includes Santiago Papasquiaro and Durango 1:250000 scale maps. Geology modified from: Mungía-Rojas *et al.* (1998), Mungía-Rojas *et al.* (2000), Ferrari *et al.* (2005), Nieto-Samaniego *et al.* (2005), SGM (2007). Segmented gray lines delimitate the influence zone of the San Luis-Tepehuanes fault system in this region.

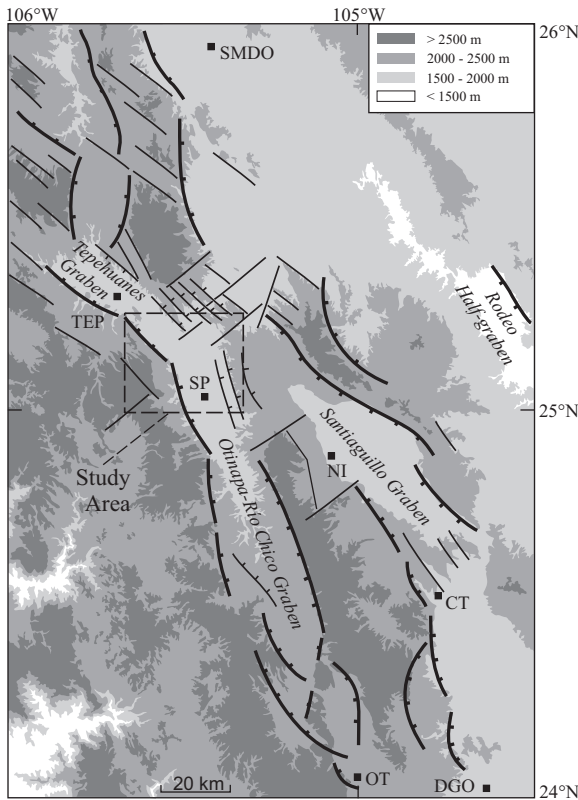


Figure 3. Elevation map of the region between Durango (DGO) and Santa María del Oro (SMDO). The principal faults that control the depressions in the region are shown; thinner lines represent the secondary structures. The most notorious depressions are the Tepehuanes graben, the Rodeo half graben, the Santiago graben and the Río Chico-Otinapa graben. The rectangle in segmented line delimits the study area of the present work. Other important cities in the region: Santiago Papasquiaro (SP), Tepehuanes (TEP), Nuevo Ideal (NI), Canatlán (CT) and Otinapa (OT).

includes Paleozoic to Quaternary rocks (Figure 2). Gneiss and schist, with a metamorphic age of ~ 252 Ma (Ar-Ar on muscovite, Iriondo *et al.*, 2003), crop out ~ 100 km to the east-southeast of Santiago Papasquiaro, and schist with a metamorphic age of 326 ± 26 Ma (K-Ar, Araujo-Mendieta and Arenas-Partida, 1986) crops out ~ 100 km to the north. Unconformably overlying the Paleozoic units are clastic and carbonate Jurassic and Cretaceous marine rocks (Zaldivar and Garduño, 1984; Aranda-García *et al.*, 1987; Contreras-Montero *et al.*, 1988; Córdoba, 1988) that were folded and thrusted during the Laramide Orogeny (Nieto-Samaniego *et al.*, 2005). These Mesozoic rocks are covered by continental conglomerates, Eocene to Miocene mainly acid to intermediate volcanic rocks of the SMOc, and Oligocene-Miocene to Pleistocene basic volcanic rocks (McDowell and Keizer, 1977; Swanson *et al.*, 1978; McDowell and Clabaugh, 1981; Córdoba, 1988; Aguirre-Díaz and McDowell, 1991; Mungía-Rojas *et al.*, 2000; Luhr *et al.*, 2001; Ferrari *et al.*, 2005; Nieto-Samaniego *et al.*, 2005; Solé *et al.*, 2007; Nieto-Samaniego *et al.*, 2012). Miocene to Quaternary alluvial and lacustrine deposits fill

continental basins, and Quaternary alkaline basalts top the lithologic column (Figure 2) (Nieto-Samaniego *et al.*, 2005).

The Mesa Central has undergone extension since the late Eocene (Nieto-Samaniego *et al.*, 2005). Previous studies have defined two main events in this region: the first one occurred in early-late Oligocene and the second one in late Miocene. These events are characterized by the development of high angle normal faults that formed graben-type tectonic depressions (Figures 1 and 3) (Aguirre-Díaz and McDowell, 1993; Aranda-Gómez *et al.*, 1997; Henry and Aranda-Gómez, 2000; Luhr *et al.*, 2001; Ferrari *et al.*, 2005; Nieto-Samaniego *et al.*, 2005, 2012). Although the timing of the regional extension is generally known, information about the age, geometry and kinematics of individual grabens and half grabens in the region is scarce, with the exception of the Santiago graben (Nieto-Samaniego *et al.*, 2012), the Rodeo half-graben (Luhr *et al.*, 2001) and the southernmost part of the Río Chico-Otinapa graben (Aranda-Gómez *et al.*, 1997; Henry and Aranda-Gómez, 2000).

3. Local stratigraphy

3.1. Early Eocene volcanism

3.1.1. *Antigua ignimbrite*

The pyroclastic deposits located at the bottom of the stratigraphic sequence are named in the present work as *Antigua ignimbrite*. This unit crops out in the northern part of the Santiago Papasquiaro-Los Altares highway and its base is not exposed (Figure 4, Tables 1 and 2). The *Antigua ignimbrite* unconformably underlies the El Cazadero andesite. A U-Pb age of $51.75 +0.35/-0.45$ Ma (Figure 5, Tables 3 and 4) was obtained by LA-ICP-MS on zircons of a representative sample of this unit (*Fres-b*). We interpret this age as the crystallization time of magmatic zircons that should be very close to the time of rock emplacement (cooling), because the date was obtained from the younger coherent group of concordant ages obtained from the border of zircons. The *Antigua ignimbrite* has similar lithological characteristics and equivalent stratigraphic position as rocks reported by Aguirre-Díaz and McDowell (1991) in the Nazas region, east of the study area (Figure 2). The volcanic sequence near Nazas consists of silicic pyroclastic rocks, intermediate lava flows and domes, with ages between 48.8 ± 3 and 40.3 ± 1 Ma (K-Ar, on plagioclase, biotite, sanidine and hornblende).

3.2. Late Eocene-early Oligocene volcanism

3.2.1. *Altamira ignimbrite*

The *Altamira ignimbrite* is a pyroclastic deposit that crops out in the eastern and southeastern parts of the study area (Figure 4, Tables 1 and 2). This unit is the A1 member of the *Altamira ignimbrite* reported by Nieto-Samaniego *et al.* (2012) in the Nuevo Ideal-Canatlán region, 40 km

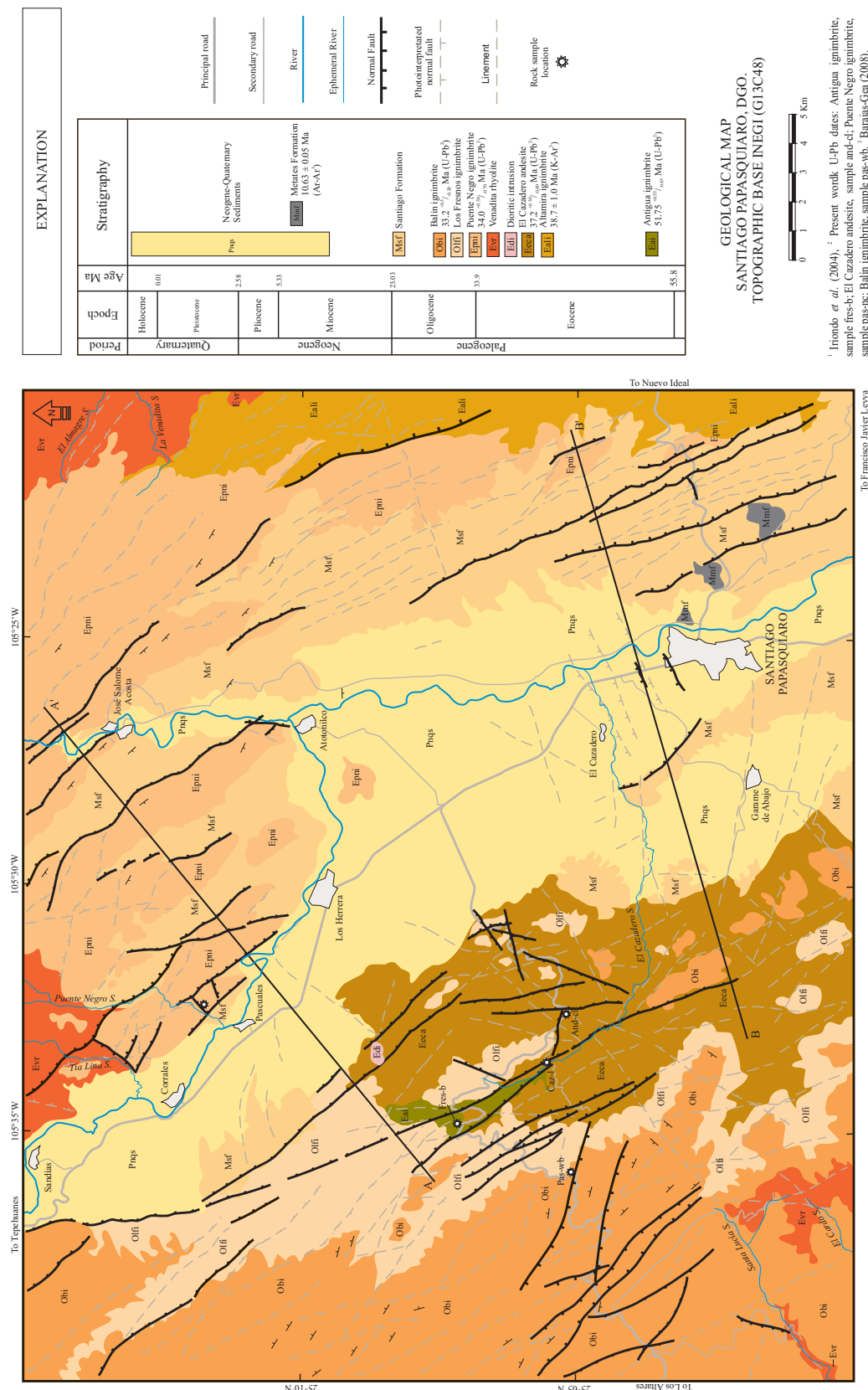


Figure 4. Geologic map of Santiago Papasquiaro, Durango State, scale 1:50,000 made on the topographic base map G13-C48 (INEGI, 2000). Shown are the isotopic ages obtained during the present work and those previously published by others. The Santiago Papasquiaro valley has a NW strike in the northern portion and a NNW strike in the center and south portions.

Table 1. Outcrop characteristics of lithostratigraphic units

Unit Name	Color	Welding	Lithics		Pumice		Phenocrysts		Matrix	Estimated Thickness (m)	Age (Ma)
			Size (cm)	Type/ Charc.	Size (cm)	Charc.	Size (mm)	Mineral			
Metates Formation	dark gray	-	-	-	-	-	-	5		10 (max.)	10.63 (Ar-Ar) (Ar-Ar)
Santiago formation	light brown-yellow	-	¼- 1 (mm)- 60 cm	subA- subR	¼- 1 (mm)- 5 cm	subA- subR	01-may	qz, Kfs >> bio	fine sand	100 (mean)	-
Balín ignimbrite	light gray-purple	mod- high	10	subA	10	modF	5	qz, Kfs, bio	ashy	200	33.2 (U-Pb)
Los Fresnos ignimbrite	red pink	mod mod- high	1 >> 3 15	aph an, rhy	1 10	notF modF	3 5	qz qz, bio	ashy ashy	150	-
Puente Negro ignimbrite	light gray	mod	3	subA	5	modF	5	qz, Kfs, bio	ashy	100	34 (U-Pb)
Venadita rhyolite	red	-	-	-	-	-	-	qz, Kfs	devitrified glass	100 (max.)	-
Dioritic intrusion	-	-	-	-	-	-	05-ago	pl, am			-
El Cazadero andesite	green purple red	-	-	-	-	-	5	am, pl	glassy	200 (max.)	35.95 37.2 (U-Pb)
Altamira ignimbrite	pink	high	5	A, mafic, aph, >> Met, Sed	8	highF		qz, Kfs, bio, hbl	glassy	80 (min.)	38.8 (K-Ar)
Antigua ignimbrite	pink	high	15	A, dark red, compact, aph	10	modF	5	qz, Kfs, bio	ashy	50 (min.)	51.75 (U-Pb)

Charc.: Characteristics.

subA: Subangular. subR: Subrounded. aph: Aphanitic. A: Angular.

qz: Quartz. Kfs: Potassium Feldspar. bio: Biotite. pl: Plagioclase. am: Amphibole. hbl: Hornblende.

mod: Moderate. modF: Moderately Flattened. notF: Not Flattened. highF: Highly Flattened.

an: Andesite fragments. rhy: Rhyolite fragments. Met: Metamorphic rock fragments. Sed: Sedimentary rock fragments.

southeast of the study area. Nieto-Samaniego *et al.* (2012) inferred that the olivine crystals (Table 2) observed in thin section must be fayalite because they appear as phenocrysts in association with quartz and K-feldspar. The Altamira ignimbrite unconformably underlies the Venadita rhyolite, Puente Negro ignimbrite and Santiago formation (Figure 4). In the Nuevo Ideal region, Nieto-Samaniego *et al.* (2012) obtained an age of 38.8 ± 1.0 Ma (K-Ar age, sanidine). This unit has lithological similarities and equivalent stratigraphic position as late Eocene-early Oligocene volcanic pulse rocks reported by Aguirre-Díaz and McDowell (1991) in the Nazas region, composed by rhyolitic domes and tuffs with ages from 34.0 ± 0.8 Ma to 29.5 ± 1.0 Ma (K-Ar ages, K-feldspar, plagioclase).

3.2.2. El Cazadero andesite

El Cazadero andesite consists of an intercalation of andesitic lava, breccia and tuff, as well as continental clastic deposits composed of andesite fragments, which crops out west of El Cazadero town, in the west-southwestern part of the study area (Figure 4). In previous studies this unit was named “andesite-andesitic breccia” (Mungía-Rojas *et al.*, 2000; Luévano-Pinedo *et al.*, 2003). General macroscopic and microscopic characteristics of lavas are shown in

Tables 1 and 2. In some outcrops along the Santiago Papasquiaro-Los Altares highway, the rock has isolated reabsorbed andesite fragments in red and pale brown flow bands. The andesitic breccia shows several tones of green with matrix-supported, subangular to subrounded volcanic rock fragments in a fine to medium grained matrix. A dark reddish brown deposit composed of coarse sandstone and shale unconformably underlies the volcanic breccia. The sandstone contains andesite fragments supported by silicic matrix. A light colored pyroclastic deposit that contains pumice and holes left by eroded pumice fragments is intercalated between clastic deposits and lavas of El Cazadero andesite. This deposit contains lithic fragments between 5 mm and 10 cm across, and isolated biotite crystals up to 5 mm in diameter. El Cazadero andesite overlies unconformably the Antigua ignimbrite. U-Pb ages of two lavas of El Cazadero andesite were obtained by laser ablation inductively coupled plasma mass spectrometer (LA-ICP-MS) on zircons. Dating results were $37.2 \pm 0.30/-0.40$ Ma (Figure 6, Tables 3 and 5) for sample *And-cl*, and $35.95 \pm 0.45/-0.5$ Ma (Figure 6, Tables 3 and 6) for sample *Caz-1*. El Cazadero andesite has similar ages and lithology as Coneto andesite of the Nuevo Ideal region, which has reported ages of 35.0 ± 0.6 Ma (Ar-Ar on plagioclase, Nieto-

Table 2. Petrographic summary of lithostratigraphic units.

Unit Name	Texture	Phenocrysts		
		%	shape	mineral
Metates Formation	fine grain, holo - hypocrystalline	< 10	subH- euH	pl, bio, px
Santiago formation		oct-40	subA- subR	
Balin ignimbrite	medium grain, hypocrystalline	20	subH- anH	qz, sa, pl >> bio
Los Fresnos ignimbrite	fine- medium grain, hypocrystalline	20- 30	subH- anH	qz, sa, bio, pl
Puente Negro ignimbrite	medium grain, hypocrystalline	10	subH	qz, sa, pl, bio
Venadita rhyolite		oct-20	subH	qz, sa, bio, pl, am, >> mag
Dioritic intrusion		20- 30	euH- subH	pl, am, qz >> ap, ms
El Cazadero andesite	medium grain hypocrystalline	< 25	subH- euH	am, pl, qz
Altamira ignimbrite			anH	qz, sa, bio, hb >> ox, ol
Antigua ignimbrite	hypocrystalline	20	anH- subH	qz, sa, bio, hb

subH: Subhedral. euH: Euhedral. anH: Anhedral. subA: Subangular. subR: Subrounded.
 pl: Plagioclase. bio: Biotite. px: Pyroxene. qz: Quartz. sa: Sanidine. am: Amphibole. mag: Magnetite. ap: Apatite. ms: Muscovite. ox: Oxides. ol: Olivine.

Samaniego *et al.*, 2012) and 40.15 +0.35/0.95 Ma (U-Pb on zircons, Nieto-Samaniego *et al.*, 2012).

3.2.3. Venadita rhyolite

In the present study the name of Venadita rhyolite was given to a group of lava domes that overlies the Altamira ignimbrite and the El Cazadero andesite (Figure 4). Outcrops of this unit can be observed in some streams like La Venadita and El Almagre in the northeast of the study area, Santa Lucia and El Cardo in the southwest, and Puente Negro and Tía Lina in the north (Figure 4). General macroscopic and microscopic characteristics are shown in Tables 1 and 2. Commonly, the rhyolite has basal vitrophyres and autobreccias as well as flow foliation. Spherulitic texture is developed in some outcrops. The matrix is devitrified and presents perlitic fractures in thin section. The Venadita rhyolite unconformably underlies the Puente Negro ignimbrite. Due to lithological features and stratigraphic position this unit has similarities with the rhyolitic dome of 34 ± 0.8 Ma reported in Nazas region (Aguirre-Díaz and McDowell, 1991). For that reason, we consider the Venadita rhyolite of late Eocene-early Oligocene age.

3.2.4. Puente Negro ignimbrite

Puente Negro ignimbrite is a massive pyroclastic deposit that crops out in the northern and northeastern parts of the study area (Figure 4, Tables 1 and 2). This unit forms large tilted plateaus in the central-northern

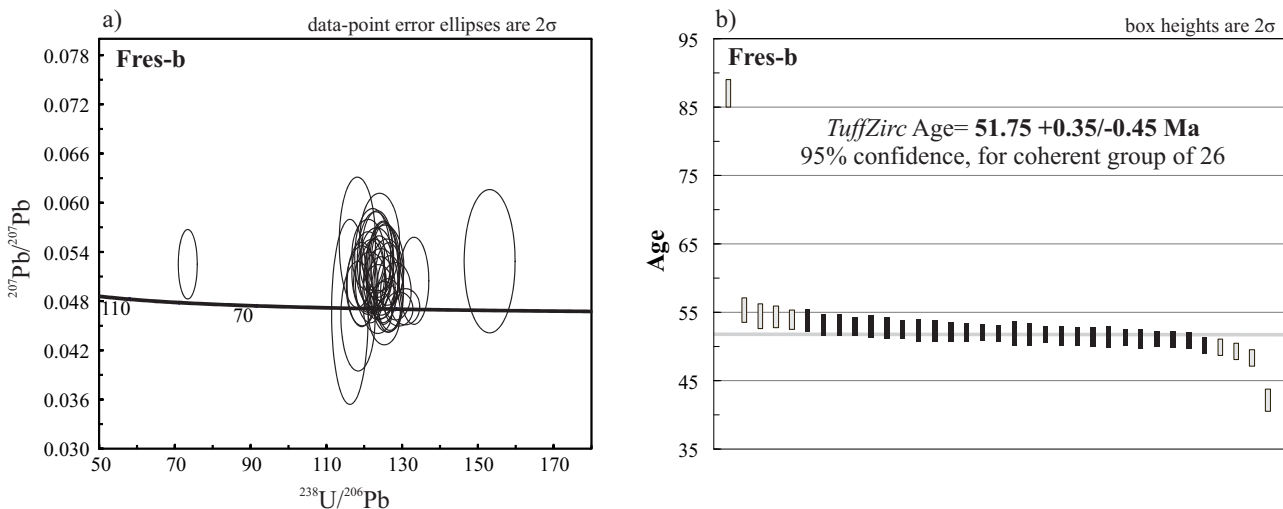


Figure 5. Zircon U-Pb data obtained by LA-ICP-MS from sample *Fres-b* of the Antigua ignimbrite. a) Tera-Wasserburg diagram showing concordant data from sample *Fres-b*. Although many of the ellipses touch the concordant curve (which means that they could be considered concordant data), there are some ellipses that do not. Part of this problem is related to the lack of common lead values (as discussed in the introduction), as well as problems related to the fact that ablation (23 microns spot) took place probably in several layers (outer and inner layers) of the zircon that could be slightly different in age (therefore, different isotopic composition is mixed during analysis). b) Mean weight age diagram for this sample.

Table 3. Results of the U-Pb isotopic dating.

Unit Name	Sample	Location	Rock type	$^{206}\text{Pb}/^{238}\text{U}$ mean age (Ma)	Confidence %	# of Spots
Balín Ignimbrite	Pas-wb	105.59° E, 25.08° N	Ignimbrite	33.2 +0.50/-0.20	95	27
Puente Negro Ignimbrite	Pas-nc	105.54° E, 25.19° N	Ignimbrite	34.0 +0.50/-0.70	94.3	14
El Cazadero Andesite	Caz-l	105.56° E, 25.09° N	Andesite	35.95 +0.45/-0.5	96.1	12
El Cazadero Andesite	And-cl	105.54° E, 25.08° N	Andesite	37.2 +0.30/-0.40	95	33
Antigua Ignimbrite	Fres-b	105.57° E, 25.11° N	Ignimbrite	51.75 +0.34/-0.45	95	26
--	Gm-26	104.79° E, 24.93° N	Rhyolite	56.4 +0.50/-0.70	97.8	13

part of the area (Figures 3 and 4). The Puente Negro ignimbrite overlies unconformably the Altamira ignimbrite and Venadita rhyolite, and underlies unconformably the Santiago formation and the Neogene-Quaternary continental sediments. A U-Pb age of 34.0 +0.50/-0.70 Ma (Figure 7, Tables 3 and 7) was obtained from a representative sample (*Pas-nc*). This unit is considered part of the late Eocene-early Oligocene volcanic pulse.

3.2.5. *Los Fresnos ignimbrite*

Los Fresnos ignimbrite is a set of pyroclastic deposits that crop out west and northwest of Santiago Papasquiaro, and can be observed along the Santiago Papasquiaro-Los Altares highway (Figure 4, Tables 1 and 2). They have been grouped previously with other volcanic deposits and named as “rhyolitic tuff-ignimbrite” by Luévan-Pinedo *et al.* (2003). In the bottom of the *Los Fresnos ignimbrite* there are a series of pyroclastic-flow and fall deposits, with a total thickness of 2 m. Individual layers are red and yellow and have thicknesses of less than 5 cm. *Los Fresnos ignimbrite* overlies unconformably the Antigua ignimbrite, the El Cazadero andesite and the Venadita rhyolite, and underlies conformably the Balín ignimbrite. *Los Fresnos ignimbrite* has not been dated. However, its stratigraphic position indicates an early Oligocene age, including this unit as part of the late Eocene-early Oligocene ignimbritic pulse (Figure 4).

3.2.6. *Balín ignimbrite*

The name *Balín ignimbrite* was given to a unit composed of pyroclastic deposits that crop out in the western sector of the study area, along the Santiago Papasquiaro-Los Altares highway (Figure 4, Tables 1 and 2). In previous studies these rocks were grouped with other deposits and were named generically as “rhyolitic tuff-ignimbrite” (Luévan-Pinedo *et al.*, 2003). In some outcrops, these deposits show pseudo-stratification and poorly developed columnar jointing. In the uppermost portion of the deposit are “pumice holes” up to 10 cm long, which are the voids left by eroded pumice fragments. Near the base of this unit, lithic fragments are bigger. The *Balín ignimbrite* overlies conformably *Los Fresnos ignimbrite* and discordantly the *El Cazadero*

andesite. The U-Pb age obtained from the sample *Pas-wb* is 33.2 +0.50/-0.20 Ma (Figure 8, Tables 3 and 8). This dating places the *Balín ignimbrite* in the early Oligocene. Considering this age, the *Balín ignimbrite* is grouped within the late Eocene-early Oligocene ignimbritic pulse.

3.2.7. *Santiago formation*

The *Santiago formation* is the name proposed for epiclastic light brown-yellowish deposits of medium to coarse sand, gravel and conglomerate that crop out in the eastern, northern and western borders of the *Santiago Papasquiaro* valley (Figure 4, Tables 1 and 2). These deposits were named in previous works as “rhyolitic breccia-rhyolitic tuff” (Luévan-Pinedo *et al.*, 2003). The most accessible outcrops are along the *Santiago Papasquiaro-Nuevo Ideal* highway as well as along the *Santiago Papasquiaro-Garame de Abajo* road (Figure 4). The *Santiago formation* includes intercalations of continental deposits of sand and conglomerates that are moderately lithified. In the southernmost outcrops these strata are composed of fragments that range in size from medium to coarse sand. Interbedded with the fine grained deposits are some lenticular deposits where fragment size increases. In the northernmost deposits of this unit the fragments are almost 60 cm. The source of these deposits probably was north of the study area because the clasts size increases toward the north. The *Santiago formation* overlies unconformably the *Puente Negro ignimbrite* and underlies unconformably basalt flows equivalent to the *Metates Formation*. This unit has similar lithological features and stratigraphic position as the *Santa Inés Formation* previously reported in *Nazas* by Aguirre-Díaz and McDowell (1991); these authors also described in the *Nazas* area 24 Ma mafic lavas overlying the *Santa Inés Formation*; mafic lavas of similar age had not been found in the *Santiago Papasquiaro* region. Taking into account its stratigraphic position, we propose a late Oligocene age for the *Santiago Formation* (Figure 4).

3.3. Miocene

3.3.1. *Basalt equivalent to the Metates Formation*

The *Metates Formation* was defined by Córdoba (1963)

Table 4. LA-ICP-MS U-Pb zircon data from sample Fres-b of the Antigua ignimbrite.

Spot number	U (ppm)	Th (ppm)	Th/U	$^{207}\text{Pb}/^{206}\text{Pb}$	$\pm 1\sigma$	$^{207}\text{Pb}/^{235}\text{U}$	$\pm 1\sigma$	$^{206}\text{Pb}/^{238}\text{U}$	$\pm 1\sigma$	$^{208}\text{Pb}/^{232}\text{Th}$	$\pm 1\sigma$	Rho	CORRECTED RATIOS				CORRECTED AGES (Ma)					
													$^{206}\text{Pb}/^{238}\text{U} \pm 1\sigma$				$^{207}\text{Pb}/^{206}\text{Pb} \pm 1\sigma$					
35	866	346	0.37	0.052586	0.003557	0.0476	0.00371	0.00653	0.00012	0.00205	0.00004	0.52	42	0.8	47	4	323	147	41.3	0.8	42	1
51	643	633	0.92	0.05047	0.00217	0.05205	0.00232	0.00751	0.00009	0.00233	0.00005	0.26	48.2	0.6	52	2	217	99	47	1	48	1
30	1701	1547	0.85	0.04731	0.0009	0.04976	0.00112	0.00764	0.00009	0.00231	0.00004	0.53	49.1	0.6	49	1	65	41	46.6	0.8	49	1
22	1939	2271	1.09	0.04703	0.00085	0.05018	0.00106	0.00774	0.00009	0.00238	0.00004	0.52	49.7	0.6	50	1	51	38	48	0.8	50	1
20	856	707	0.77	0.0492	0.00143	0.0527	0.00167	0.00779	0.0001	0.0024	0.00004	0.4	50	0.6	52	2	157	63	48.5	0.8	50	1
44	309	207	0.62	0.04898	0.00186	0.05312	0.00212	0.00789	0.00009	0.00257	0.00007	0.31	50.7	0.6	53	2	147	83	52	1	51	1
14	261	179	0.64	0.04967	0.00223	0.05415	0.00276	0.00791	0.0001	0.0025	0.00003	0.33	50.8	0.6	54	3	180	102	50.4	0.7	51	1
27	497	390	0.73	0.04747	0.00133	0.05186	0.0016	0.00792	0.0001	0.00242	0.00005	0.42	50.9	0.6	51	2	73	59	49	1	51	1
54	516	474	0.86	0.05153	0.00165	0.05612	0.00196	0.00793	0.00011	0.00247	0.00005	0.4	50.9	0.7	55	2	265	74	50	1	51	1
38	397	292	0.68	0.0522	0.00214	0.05734	0.00247	0.00796	0.0001	0.00248	0.00005	0.31	51.1	0.6	57	2	294	89	50	1	51	1
28	501	390	0.72	0.04653	0.00158	0.05101	0.00188	0.00798	0.00011	0.00241	0.00005	0.39	51.2	0.7	51	2	25	65	49	1	51	1
45	268	162	0.56	0.05215	0.00209	0.05715	0.00246	0.00797	0.00013	0.00238	0.00008	0.37	51.2	0.8	56	2	292	87	48	2	51	1
15	504	416	0.77	0.0514	0.00255	0.05665	0.00317	0.00799	0.0001	0.00251	0.00003	0.3	51.3	0.7	56	3	259	114	50.8	0.6	51	1
46	395	349	0.82	0.05155	0.00253	0.05654	0.00288	0.008	0.00011	0.00246	0.00005	0.27	51.4	0.7	56	3	266	107	50	1	51	1
40	484	345	0.66	0.05034	0.00166	0.05536	0.00201	0.00804	0.00012	0.00252	0.00005	0.42	51.6	0.8	55	2	211	72	51	1	52	1
42	514	425	0.77	0.04964	0.00154	0.05489	0.00182	0.00804	0.0001	0.00252	0.00005	0.35	51.6	0.6	54	2	178	68	51	1	52	1
39	187	106	0.53	0.05552	0.00243	0.06091	0.00287	0.00806	0.00014	0.00243	0.00007	0.36	51.7	0.9	60	3	420	94	49	1	52	1
29	415	310	0.69	0.05201	0.00161	0.05801	0.00195	0.00807	0.0001	0.00248	0.00007	0.39	51.8	0.6	57	2	286	66	50	1	52	1
26	432	288	0.62	0.04909	0.00137	0.05467	0.00169	0.00808	0.00011	0.0026	0.00005	0.43	51.9	0.7	54	2	152	61	52	1	52	1
10	830	725	0.81	0.04667	0.00107	0.05213	0.00135	0.00809	0.0001	0.00246	0.00004	0.47	51.9	0.6	52	1	32	45	49.7	0.8	52	1
48	305	192	0.59	0.054	0.00205	0.05927	0.0024	0.0081	0.00011	0.00268	0.00007	0.35	52	0.7	58	2	371	82	54	1	52	1
8	375	284	0.71	0.05269	0.00174	0.05857	0.00212	0.00811	0.00012	0.00252	0.00005	0.41	52.1	0.8	58	2	315	72	51	1	52	1
23	225	128	0.53	0.05282	0.00248	0.05931	0.00294	0.00813	0.00013	0.00254	0.00007	0.32	52.2	0.8	59	3	321	100	51	1	52	1
21	294	199	0.63	0.05102	0.00184	0.057	0.0022	0.00814	0.00011	0.00247	0.00007	0.36	52.3	0.7	56	2	242	77	50	1	52	1
47	226	140	0.58	0.05329	0.00245	0.05962	0.00229	0.00818	0.00013	0.00258	0.00008	0.33	52.5	0.8	59	3	341	99	52	2	53	1
33	252	201	0.74	0.05041	0.00207	0.05654	0.00243	0.00822	0.00011	0.00251	0.00006	0.3	52.8	0.7	56	2	214	88	51	1	53	1
24	339	238	0.65	0.04986	0.00199	0.05751	0.00244	0.00837	0.00012	0.00254	0.00006	0.34	53.7	0.8	57	2	188	86	51	1	54	1
17	559	296	0.49	0.05028	0.00151	0.05676	0.00119	0.00823	0.00012	0.00255	0.00005	0.44	52.8	0.8	56	2	208	70	51	1	53	1
18	223	172	0.72	0.05142	0.00206	0.05802	0.00248	0.00826	0.00012	0.00253	0.00006	0.35	53	0.8	57	2	260	88	51	1	53	1
53	437	299	0.64	0.05363	0.00177	0.06092	0.00218	0.00826	0.00012	0.00255	0.00005	0.39	53	0.8	60	2	356	75	51	1	53	1
12	112	77	0.64	0.05516	0.00325	0.06302	0.00387	0.00846	0.00014	0.00277	0.00008	0.28	54.3	0.9	62	4	419	132	56	2	54	1
9	183	138	0.7	0.04668	0.00461	0.05537	0.00582	0.0086	0.00015	0.00274	0.00017	0.19	55.2	0.9	55	6	33	193	55	3	55	1
52	273	118	0.4	0.05249	0.00173	0.09841	0.00353	0.01362	0.00019	0.00424	0.00011	0.39	87	1	95	3	307	75	86	2	87	1

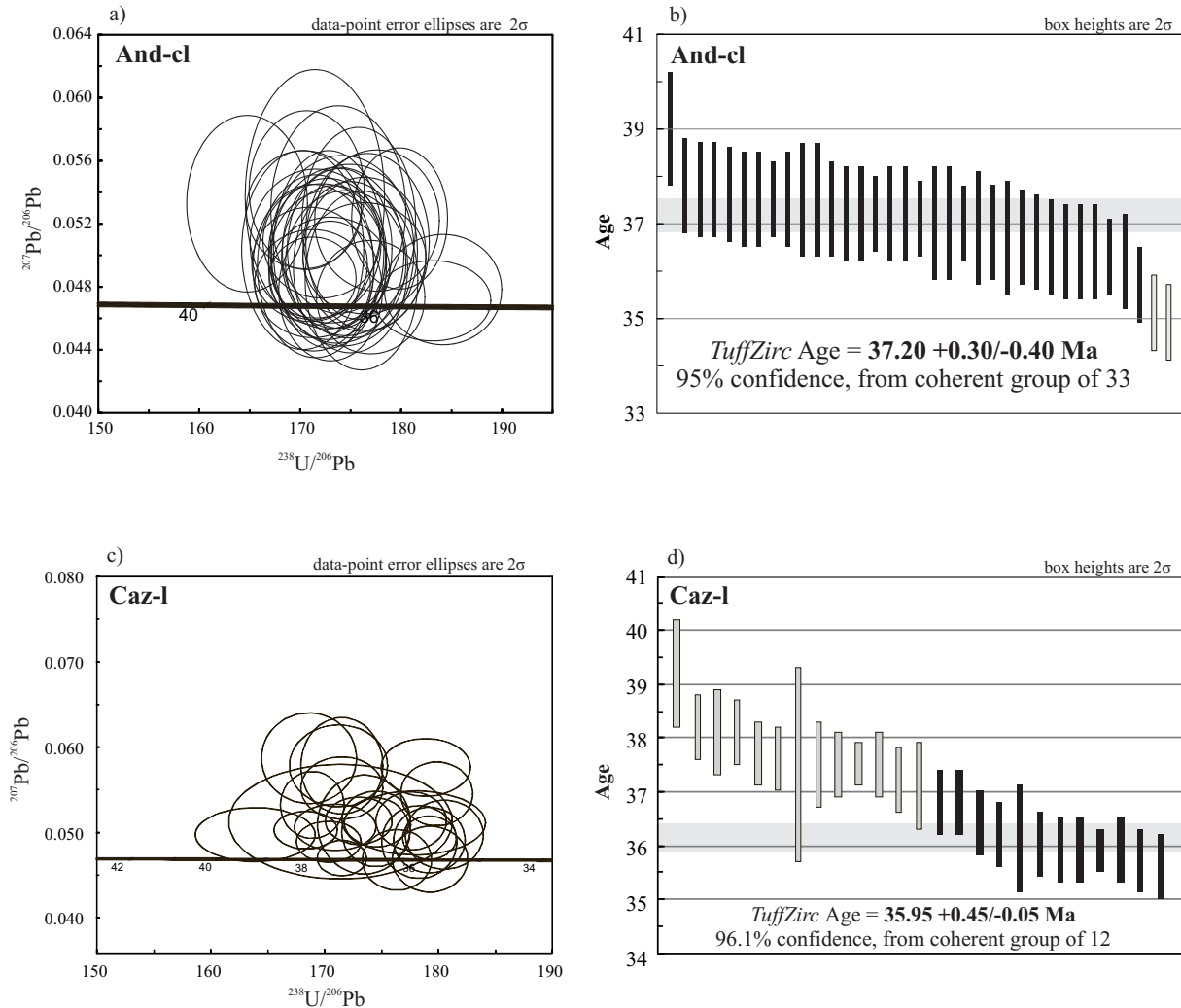


Figure 6. Zircon U-Pb data obtained by LA-ICP-MS for samples *And-cl* and *Caz-l* of El Cazadero andesite. a) Tera-Wasserburg diagram showing concordant data from sample *And-cl*. b) Mean weight age diagram for this sample. c) Tera-Wasserburg diagram showing concordant data from sample *Caz-l*. d) Mean weight age diagram for this sample.

west of Durango City, around 130 km to the south-southeast of Santiago Papasquiaro. Equivalent basalts mapped in the study area consist of basaltic flows and dikes, which overlie and/or intrude the late Eocene-early Oligocene ignimbritic sequence. Small basalt flows crop out east of Santiago Papasquiaro (Figure 4). Also, some dikes and small flows crop out along the Santiago Papasquiaro-Nuevo Ideal highway and the Santiago Papasquiaro-Francisco Javier Leyva road. These lava flows usually present basal and upper breccias, and some glomerophenocrysts of *ca.* 15 mm (Tables 1 and 2). The basalts equivalent to the Metates Formation overlie unconformably the Santiago formation and are intercalated with Neogene-Quaternary unconsolidated deposits (Figure 4). Iriondo *et al.* (2004) obtained Ar-Ar isochron and plateau-like ages of 10.63 ± 0.05 Ma and 10.95 ± 0.02 Ma from one sample of these lavas, locating this unit at the base of the late Miocene.

3.3.2. Neogene-Quaternary sediments

The Santiago Papasquiaro half-graben topographic depression is filled by sand, conglomerate and lacustrine deposits (Figure 4). The lacustrine deposits are carbonate rich, light colored and composed mainly of fine material with isolated lithics, crystals and pumice, which are less than 5 mm size. They are intercalated with fine to coarse grain sand deposits that show cross bedding. Layering has variable thickness from 5 to 20 cm. In the Neogene-Quaternary sediments there also are clast-supported conglomerates composed of subangular to subrounded volcanic and metamorphic rocks of 2 mm to 15 cm size. These conglomerates are intercalated with other deposits composed of isolated volcanic clasts of ~20 cm and lacustrine fragments, all supported by a clayey matrix. Other deposits are composed of medium grain red sands with lacustrine deposit fragments. These sands show incipient stratification, in some places clay matrix is present. The

Table 5. LA-ICP-MS U-Pb zircon data from sample And-c1 from El Cazadero andesite.

Spot number	U (ppm)	Th (ppm)	Th/U	$^{207}\text{Pb}/^{206}\text{Pb}$	$^{207}\text{Pb}/^{235}\text{U}$	$\pm 1\sigma$	$^{206}\text{Pb}/^{238}\text{U}$	$\pm 1\sigma$	CORRECTED RATIOS				CORRECTED AGES (Ma)									
									$^{206}\text{Pb}/^{235}\text{U}$	$\pm 1\sigma$	$^{208}\text{Pb}/^{232}\text{Th}$	$\pm 1\sigma$	$^{206}\text{Pb}/^{238}\text{U}$	$\pm 1\sigma$	$^{207}\text{Pb}/^{206}\text{Pb}$	$\pm 1\sigma$						
27	1212	1181	0.89	0.04782	0.00143	0.03583	0.00117	0.00543	0.00007	0.00166	0.00003	0.4	34.9	0.4	36	1	90	65	33.5	0.6	35	0
50	1798	994	0.5	0.04711	0.00104	0.03539	0.00089	0.00546	0.00007	0.00177	0.00004	0.48	35.1	0.4	35.3	0.9	55	46	35.7	0.8	35	0
17	938	484	0.47	0.05233	0.00183	0.04029	0.00148	0.00556	0.00006	0.00187	0.00007	0.31	35.7	0.4	40	1	300	72	38	1	36	0
41	537	293	0.5	0.0522	0.00183	0.04034	0.00152	0.00563	0.00008	0.00183	0.00005	0.37	36.2	0.5	40	1	294	74	37	1	36	1
47	1019	652	0.58	0.04734	0.00147	0.03674	0.00123	0.00565	0.00007	0.00174	0.00003	0.37	36.3	0.4	37	1	66	62	35.1	0.6	36	0
33	727	517	0.65	0.04981	0.00144	0.03874	0.00125	0.00567	0.00008	0.00175	0.00004	0.44	36.4	0.5	39	1	186	64	35.3	0.8	36	1
35	405	318	0.71	0.05085	0.00229	0.03938	0.00186	0.00566	0.00008	0.00177	0.00004	0.3	36.4	0.5	39	2	234	95	35.7	0.8	36	1
12	495	271	0.5	0.05005	0.002	0.03898	0.00165	0.00567	0.00008	0.00186	0.00005	0.33	36.4	0.5	39	2	197	83	38	1	36	1
48	614	430	0.64	0.0484	0.00232	0.0379	0.00209	0.00568	0.00007	0.0018	0.00004	0.37	36.5	0.5	38	2	119	98	36.3	0.7	37	1
51	541	324	0.55	0.05202	0.00249	0.04048	0.00222	0.00569	0.00007	0.00179	0.00002	0.31	36.6	0.5	41	2	286	100	36.1	0.4	37	1
20	1001	542	0.49	0.05026	0.00225	0.03961	0.00218	0.00572	0.00009	0.0018	0.00002	0.42	36.7	0.6	39	2	207	97	36.4	0.5	37	1
15	548	477	0.79	0.04924	0.00222	0.0388	0.00207	0.00571	0.00008	0.00181	0.00002	0.39	36.7	0.5	39	2	159	92	36.5	0.5	37	1
38	553	339	0.56	0.0495	0.00188	0.03913	0.00158	0.00573	0.00008	0.00184	0.00004	0.34	36.8	0.5	39	2	172	81	37.2	0.8	37	1
52	488	331	0.62	0.05028	0.00247	0.03938	0.00236	0.00574	0.00001	0.00181	0.00003	0.4	36.9	0.6	40	2	208	103	36.6	0.6	37	1
21	397	200	0.46	0.05043	0.00207	0.03991	0.00172	0.00575	0.00007	0.00194	0.00005	0.31	37	0.4	40	2	215	89	39	1	37	0
23	489	291	0.54	0.0529	0.00269	0.04197	0.00253	0.00575	0.00009	0.0018	0.00002	0.33	37	0.6	42	2	325	110	36.4	0.5	37	1
28	415	208	0.46	0.05	0.00228	0.03968	0.00217	0.00576	0.00009	0.00182	0.00003	0.35	37	0.6	40	2	195	99	36.7	0.5	37	1
34	586	376	0.58	0.0499	0.00185	0.03953	0.00154	0.00577	0.00007	0.00189	0.00005	0.31	37.1	0.4	39	2	190	80	38	1	37	0
30	678	369	0.5	0.04773	0.00181	0.03788	0.00151	0.00578	0.00007	0.00176	0.00004	0.31	37.2	0.4	38	1	86	79	35.5	0.8	37	0
32	456	244	0.49	0.04938	0.00193	0.03913	0.00161	0.00579	0.00008	0.00186	0.00005	0.31	37.2	0.5	39	2	166	85	38	1	37	1
36	508	336	0.6	0.05037	0.00256	0.04018	0.00231	0.00579	0.00007	0.00182	0.00003	0.31	37.2	0.5	40	2	212	107	36.8	0.5	37	1
53	561	370	0.6	0.0501	0.00195	0.0398	0.00164	0.00579	0.00008	0.00181	0.00004	0.33	37.1	0.4	39	2	190	80	36.6	0.6	37	1
16	668	490	0.67	0.04906	0.00137	0.03914	0.00121	0.00578	0.00008	0.00179	0.00004	0.43	37.2	0.5	39	1	151	59	36.1	0.8	37	1
9	741	719	0.88	0.05091	0.00148	0.04056	0.00131	0.00581	0.00008	0.00179	0.00004	0.44	37.3	0.5	40	1	237	64	36.1	0.8	37	1
26	1721	1073	0.57	0.04853	0.00107	0.03895	0.00096	0.00584	0.00006	0.00198	0.00004	0.45	37.5	0.4	38.8	0.9	125	49	40	0.8	38	0
39	861	394	0.42	0.0482	0.0014	0.03873	0.00123	0.00584	0.00008	0.00187	0.00005	0.41	37.5	0.5	40	2	200	82	36.6	0.8	37	1
10	377	325	0.78	0.0493	0.00237	0.03943	0.00136	0.00583	0.00008	0.00176	0.00004	0.26	37.5	0.5	43	2	162	100	35.5	0.8	38	1
44	431	217	0.46	0.04921	0.00216	0.03961	0.00203	0.00584	0.00008	0.00185	0.00003	0.34	37.5	0.5	40	1	158	92	37.3	0.6	38	1
11	427	253	0.54	0.05368	0.00331	0.04317	0.00301	0.00583	0.00001	0.00183	0.00003	0.31	37.5	0.6	43	3	358	126	36.9	0.6	38	1
8	638	548	0.78	0.04942	0.00148	0.0399	0.00132	0.00585	0.00008	0.0018	0.00004	0.43	37.6	0.5	40	1	109	62	38	1	38	1
18	501	330	0.6	0.05289	0.00153	0.04294	0.00136	0.00587	0.00008	0.00191	0.00005	0.41	37.7	0.5	43	1	324	62	39	1	38	1
24	486	276	0.52	0.05413	0.00206	0.04357	0.00175	0.00586	0.00008	0.00179	0.00004	0.32	37.7	0.5	43	2	376	81	36.1	0.8	38	1
42	879	614	0.63	0.05033	0.00258	0.04076	0.00245	0.00587	0.00009	0.00185	0.00003	0.48	37.8	0.5	41	2	210	108	37.4	0.5	38	1
14	298	138	0.42	0.05327	0.00229	0.04449	0.00203	0.00607	0.00009	0.00201	0.00007	0.34	39	0.6	44	2	340	87	41	1	39	1

Table 6. LA-ICP-MS zircon data from sample Caz-1 of El Cazadero andesite.

Spot number	U (ppm)	Th (ppm)	Th/U	$^{207}\text{Pb}/^{206}\text{Pb}$		$\pm 1\sigma$	$^{207}\text{Pb}/^{235}\text{U}$		$\pm 1\sigma$	$^{206}\text{Pb}/^{238}\text{U}$		$\pm 1\sigma$	$^{208}\text{Pb}/^{232}\text{Th}$		$\pm 1\sigma$	$^{206}\text{Pb}/^{238}\text{U}$		$\pm 1\sigma$	$^{207}\text{Pb}/^{235}\text{U}$		$\pm 1\sigma$	$^{208}\text{Pb}/^{232}\text{Th}$		CORRECTED AGES (Ma)		
				$^{207}\text{Pb}/^{206}\text{Pb}$	$^{207}\text{Pb}/^{206}\text{Pb}$		$^{207}\text{Pb}/^{235}\text{U}$	$^{207}\text{Pb}/^{235}\text{U}$		$^{206}\text{Pb}/^{238}\text{U}$	$^{206}\text{Pb}/^{238}\text{U}$		$^{208}\text{Pb}/^{232}\text{Th}$	$^{208}\text{Pb}/^{232}\text{Th}$		$^{207}\text{Pb}/^{235}\text{U}$	$^{207}\text{Pb}/^{235}\text{U}$		$^{208}\text{Pb}/^{232}\text{Th}$	$^{208}\text{Pb}/^{232}\text{Th}$		$^{207}\text{Pb}/^{235}\text{U}$	$^{208}\text{Pb}/^{232}\text{Th}$	$\pm 1\sigma$	$\pm 1\sigma$	
17	727	383	0.58	0.0497	0.00166	0.03796	0.00141	0.00554	0.00004	0.00001	0.28	35.6	0.3	38	1	181	74	35.3	0.3	36	0	36	0	36	0	
33	563	314	0.61	0.0545	0.00153	0.04168	0.00112	0.00556	0.00004	0.00003	0.22	35.7	0.3	41	1	392	64	36.1	0.6	36	0	36	0	36	0	
18	638	667	1.15	0.04907	0.00157	0.03788	0.00124	0.00558	0.00004	0.00003	0.21	35.9	0.3	38	1	151	75	33.9	0.6	36	0	36	0	36	0	
39	776	617	0.87	0.04935	0.00104	0.03797	0.00083	0.00558	0.00003	0.00003	0.27	35.9	0.2	37.8	0.8	164	48	34.7	0.6	36	0	36	0	36	0	
10	563	382	0.74	0.05761	0.00138	0.04455	0.00114	0.00559	0.00005	0.00003	0.35	35.9	0.3	44	1	515	52	34.1	0.6	36	0	36	0	36	0	
42	896	683	0.84	0.04683	0.00158	0.03602	0.00137	0.00558	0.00004	0.00002	0.32	35.9	0.3	36	1	40	69	35.9	0.5	36	0	36	0	36	0	
41	585	329	0.62	0.04884	0.00174	0.03777	0.00149	0.00561	0.00004	0.00002	0.24	36	0.3	38	1	140	79	35.9	0.3	36	0	36	0	36	0	
12	609	427	0.77	0.05108	0.00153	0.03925	0.0013	0.00562	0.00008	0.00003	0.43	36.1	0.5	39	1	244	68	34.1	0.6	36	1	36	1	36	1	
36	580	406	0.77	0.05132	0.00139	0.03988	0.00111	0.00563	0.00004	0.00003	0.23	36.2	0.3	40	1	255	61	34.5	0.6	36	0	36	0	36	0	
11	529	323	0.67	0.04675	0.00145	0.03678	0.00118	0.00567	0.00004	0.00004	0.26	36.4	0.3	37	1	36	64	32.9	0.8	36	0	36	0	36	0	
9	572	324	0.62	0.05	0.00165	0.03977	0.00134	0.00573	0.00004	0.00004	0.2	36.8	0.3	40	1	195	77	37.4	0.8	37	0	37	0	37	0	
14	834	574	0.76	0.05153	0.00134	0.04046	0.00109	0.00573	0.00004	0.00003	0.25	36.8	0.3	40	1	265	59	36.6	0.6	37	0	37	0	37	0	
15	596	421	0.78	0.05069	0.00237	0.04046	0.00212	0.00576	0.00006	0.00002	0.27	37.1	0.4	40	2	236	105	36.7	0.3	37	0	37	0	37	0	
8	1041	634	0.67	0.05134	0.00113	0.04086	0.00094	0.00578	0.00004	0.00003	0.29	37.2	0.3	40.7	0.9	256	51	34.5	0.6	37	0	37	0	37	0	
24	462	233	0.55	0.05518	0.00149	0.04445	0.00125	0.00583	0.00005	0.00004	0.28	37.5	0.3	44	1	420	61	37.8	0.8	38	0	38	0	38	0	
26	333	196	0.65	0.05778	0.00196	0.04619	0.00165	0.00584	0.00006	0.00004	0.31	37.5	0.4	46	2	521	75	29	1	38	0	38	0	38	0	
35	270	188	0.76	0.05778	0.00231	0.04631	0.00119	0.00583	0.00005	0.00023	0.00044	0.23	37.5	0.3	46	2	521	86	46	9	38	0	38	0		
40	511	312	0.67	0.05123	0.00274	0.04121	0.00296	0.00583	0.00014	0.00004	0.28	37.5	0.9	41	3	251	120	37.1	0.7	38	1	38	0	38	0	
16	1767	1082	0.67	0.04695	0.00085	0.03778	0.00071	0.00583	0.00003	0.00017	0.00002	0.27	37.5	0.2	37.7	0.7	47	39	34.3	0.4	38	0	38	0	38	0
34	970	554	0.63	0.05059	0.00111	0.04067	0.00095	0.00585	0.00005	0.00156	0.00003	0.34	37.6	0.3	40.5	0.9	222	51	31.5	0.6	38	0	38	0	38	0
38	1239	460	0.41	0.04889	0.00098	0.03956	0.00084	0.00587	0.00004	0.00177	0.00003	0.33	37.7	0.3	39.4	0.8	143	46	35.7	0.6	38	0	38	0	38	0
20	424	241	0.62	0.05867	0.00217	0.04763	0.00182	0.00593	0.00006	0.00185	0.00004	0.25	38.1	0.4	47	2	555	82	37.4	0.8	38	0	38	0	38	0
27	594	331	0.61	0.05319	0.0016	0.04348	0.00135	0.00592	0.00004	0.00188	0.00003	0.25	38.1	0.3	43	1	337	69	38	0.6	38	0	38	0	38	0
22	1729	1176	0.75	0.05024	0.0009	0.04112	0.00078	0.00594	0.00004	0.00179	0.00003	0.32	38.2	0.3	41	0.8	206	42	36.1	0.6	38	0	38	0	38	0
23	844	751	0.98	0.04971	0.00129	0.04172	0.00121	0.0061	0.00008	0.00187	0.00003	0.45	39.2	0.5	42	1	181	61	37.8	0.6	39	1	39	1	39	1

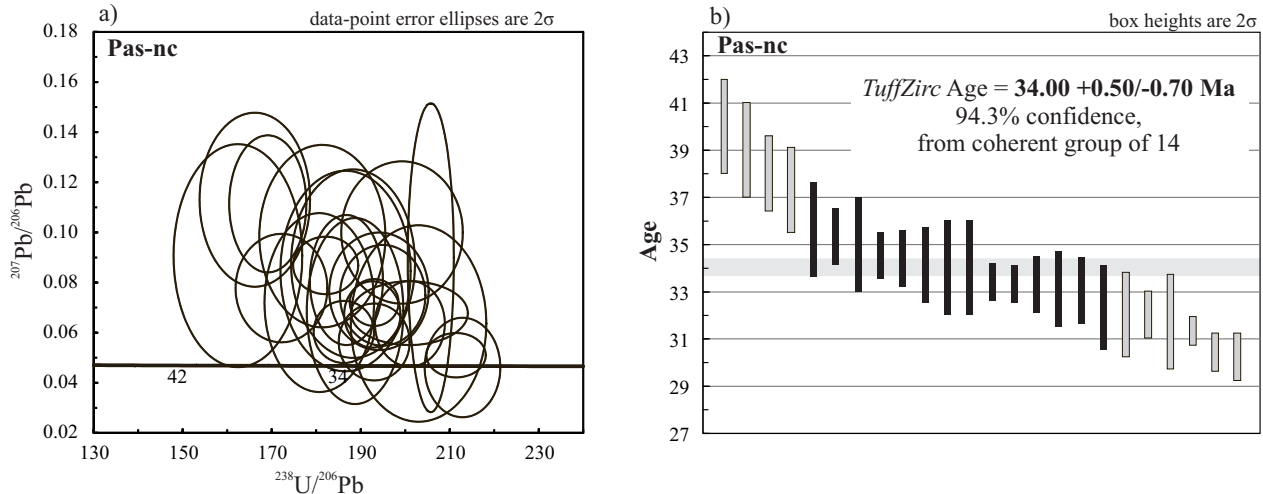


Figure 7. Zircon U-Pb data obtained by LA-ICP-MS for sample *Pas-nc* of the Puente Negro ignimbrite. a) Tera-Wasserburg diagram showing concordant data from sample *Pas-nc*. b) Mean weight age diagram for this sample.

estimated thickness for the Neogene-Quaternary sediments is around 300 m (INEGI, 1990). These deposits contain intercalated basaltic lavas (equivalent to the Metates Formation) and overlie unconformably the Santiago formation and the Puente Negro ignimbrite, showing a stratigraphic range from Neogene to Quaternary (Figure 4).

3.4. Dioritic intrusion

A dioritic intrusive neck crops out west-southwest of Los Herrera (Figure 4, Tables 1 and 2). This intrusion was reported previously by Mungía-Rojas *et al.* (2000) and Luévano-Pinedo *et al.* (2003). This body intrudes rocks of the El Cazadero andesite of late Eocene age.

4. Structure of the Santiago Papasquiaro valley

The Santiago Papasquiaro valley is formed by NNW and NW striking blocks tilted to the southwest (Figures 3, 4 and 9). The tilted blocks of the Santiago Papasquiaro valley were formed in the intersection of two major fault systems: the San Luis-Tepehuanes NW-striking fault system (SLTFS) and the Río Chico-Otinapa NNW graben (RCOG) (Figures 1 and 3) (Nieto-Samaniego *et al.*, 2005). The Tepehuanes and Santiaguillo grabens are part of the SLTFS (Figure 3) (Nieto-Samaniego *et al.*, 2012). Between the Santiaguillo and Tepehuanes grabens there is a zone with NW faults that produce elongated blocks tilted to the southwest (Figures 3, 4 and 9). The second system is formed of several NNW grabens and half grabens that form a tectonic depression that is ~150 km long and averages 10 km wide (Figure 3). The northernmost structure of the RCOG is the Santiago Papasquiaro half-graben, which is oriented N15°W and is ~40 km long and ~10 km wide. Within the study area the

master faults of both the SLTFS and RCOG are located in the western border of the Santiago Papasquiaro valley (Figures 3, 4 and 9). Those faults separate the Neogene-Quaternary sediments from the late Eocene-early Oligocene volcanic units. The estimated throw of the Santiago Papasquiaro half-graben (RCOG) is around 200 m, but considering throws of the adjacent major faults, the total throw is around 600 m (Figures 4 and 9). The throw of the SLTFS master fault is 500 m, adding the throws of the adjacent major faults, the total estimated throw reaches 800 m (Figures 4 and 9).

The average strike of the measured planes is NNW, and there is no significant difference between northern and southern portions of the measured fault planes (Figure 10). As seen in Figure 3, the average strike of SLTFS and RCOG is very similar at Santiago Papasquiaro latitude. Although the slickenlines show large dispersion, the movement is mainly normal to left oblique (Figure 10). Calculated strain tensors, using the dynamic analysis of Spang (1972), show minimum principal stress oriented 230/01 for the northern part of the study area and 244/05 for the southern part (Figure 10). We can see that inversion results are similar for both analyses, considering separately northern and southern data; this means that very similar strain tensors were obtained for both SLTFS and the Santiago Papasquiaro half-graben (Figure 10).

5. Geologic Evolution

Most of the volcanic rocks in this portion of the Mesa Central were emplaced during the Eocene and Oligocene time. Two pulses can be identified: one occurred during the Paleocene-middle Eocene and the other during the late Eocene-early Oligocene (Figure 11). From the Miocene to Recent, volcanic activity was scattered and sporadic.

Table 7 LA-ICP-MS zircon data from sample *Pas-nc* of Puente Negro ignimbrite.

Spot number	U (ppm)	Th (ppm)	Th/U	CORRECTED RATIOS			CORRECTED AGES (Ma)															
				$^{207}\text{Pb}/^{206}\text{Pb}$	$\pm 1\sigma$	$^{207}\text{Pb}/^{235}\text{U}$	$\pm 1\sigma$	$^{206}\text{Pb}/^{238}\text{U}$	$\pm 1\sigma$	Rho	$^{206}\text{Pb}/^{238}\text{Th}$	$\pm 1\sigma$	$^{207}\text{Pb}/^{235}\text{U}$	$\pm 1\sigma$	$^{207}\text{Pb}/^{206}\text{Pb}$	$\pm 1\sigma$	$^{208}\text{Pb}/^{232}\text{Th}$	$\pm 1\sigma$				
18	251	313	1.17	0.04609	0.00811	0.02985	0.00583	0.0047	0.00008	0.00166	0.0002	0.24	30.2	6	30	6	292	33	4	30	1	
34	292	351	1.13	0.05099	0.00362	0.03325	0.00264	0.0473	0.00006	0.00149	0.00002	0.21	30.4	0.4	33	3	240	157	30.1	0.4	30	0
26	224	188	0.79	0.08988	0.02517	0.06013	0.01685	0.0486	0.00005	0.00167	0.00004	0.04	31.3	0.3	59	16	1423	577	33.7	0.8	31	0
22	327	382	1.1	0.06364	0.01601	0.04322	0.01188	0.0493	0.00015	0.00151	0.00008	0.44	31.7	1	43	12	730	500	31	2	32	1
23	376	480	1.2	0.06775	0.0052	0.04648	0.00458	0.0498	0.00013	0.00152	0.00003	0.54	32	0.9	46	4	861	157	30.6	0.6	32	1
24	240	254	0.99	0.06356	0.00699	0.04358	0.00523	0.0497	0.00008	0.00153	0.00002	0.22	32	0.5	43	5	727	234	30.8	0.4	32	1
27	73	104	1.34	0.09994	0.01116	0.06914	0.00921	0.0502	0.00014	0.00147	0.00004	0.32	32.3	0.9	68	9	1623	216	29.6	0.7	32	1
10	127	113	0.83	0.07489	0.00821	0.05297	0.00633	0.0513	0.0001	0.00154	0.00003	0.32	33	0.7	52	6	1066	209	31.2	0.6	33	1
16	176	189	1.01	0.07647	0.00958	0.05432	0.00761	0.0515	0.00012	0.00155	0.00003	0.43	33.1	0.8	54	7	1107	238	31.3	0.6	33	1
36	143	87	0.57	0.05625	0.00627	0.04018	0.00473	0.0518	0.00009	0.00161	0.00004	0.23	33.3	0.6	40	5	462	233	32.6	0.7	33	1
14	184	138	0.7	0.07201	0.00382	0.05148	0.00279	0.0518	0.00006	0.00116	0.00005	0.2	33.3	0.4	51	3	986	101	32	1	33	0
15	167	125	0.7	0.06725	0.00541	0.04814	0.00419	0.0519	0.00007	0.00158	0.00002	0.27	33.4	0.4	48	4	845	157	32	0.4	33	0
41	87	79	0.85	0.08457	0.01634	0.06248	0.01329	0.0536	0.00017	0.00159	0.00005	0.42	34	1	62	13	1306	368	32	1	34	1
32	105	77	0.69	0.08752	0.01536	0.06409	0.01222	0.0531	0.00016	0.00157	0.00005	0.39	34	1	63	12	1372	328	32	1	34	1
35	92	80	0.82	0.06686	0.01516	0.05011	0.01181	0.053	0.00012	0.00161	0.00006	0.29	34.1	0.8	50	11	887	446	33	1	34	1
17	133	116	0.82	0.08098	0.0106	0.05978	0.00824	0.0535	0.0001	0.00116	0.00003	0.22	34.4	0.6	59	8	1221	242	32.3	0.7	34	1
42	131	102	0.73	0.06026	0.00506	0.04412	0.00376	0.0537	0.00008	0.00156	0.00005	0.17	34.5	0.5	44	4	613	171	32	1	35	1
21	85	105	1.15	0.0985	0.01487	0.07487	0.01291	0.0551	0.00018	0.00161	0.00004	0.33	35	1	73	12	1596	287	32.6	0.9	35	1
12	118	122	0.97	0.0868	0.00469	0.06482	0.00365	0.0549	0.00009	0.00171	0.00007	0.28	35.3	0.6	64	3	1356	97	35	1	35	1
9	198	178	0.84	0.07198	0.01458	0.05492	0.01234	0.0553	0.00015	0.00167	0.00005	0.43	35.6	1	54	12	985	435	34	1	36	1
11	65	43	0.62	0.07776	0.00884	0.06226	0.00765	0.0581	0.00014	0.00174	0.00004	0.28	37.3	0.9	61	7	1141	214	35.2	0.9	37	1
28	80	82	0.96	0.11136	0.01117	0.09078	0.00988	0.0591	0.00012	0.00171	0.00004	0.19	38	0.8	88	9	1822	181	34.5	0.7	38	1
40	53	66	1.17	0.11301	0.01418	0.09374	0.01329	0.0602	0.00018	0.00173	0.00005	0.36	39	1	91	12	1848	216	35	1	39	1
8	77	47	0.57	0.09071	0.01817	0.077	0.01721	0.0616	0.00022	0.00182	0.00007	0.38	40	1	75	16	1441	404	37	1	40	1

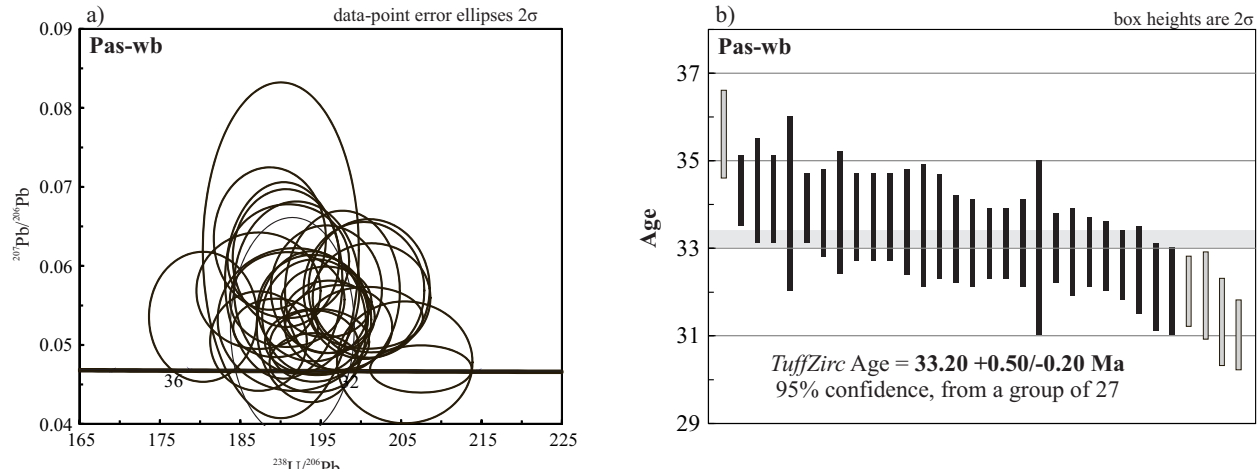


Figure 8. Zircon U-Pb data obtained by La-ICP-MS for sample *Pas-wb* of the Balín ignimbrite. a) Tera-Wasserburg diagram showing concordant data from sample *Pas-wb*. b) Mean weight age diagram for this sample.

The Paleocene-middle Eocene event is characterized by volcanism that ranges in composition from rhyolite to andesite. Rocks of this volcanic pulse have been reported in Durango (McDowell and Keizer, 1977), Nazas (Aguirre-Díaz and McDowell, 1991), Santiago Papasquiaro and Nuevo Ideal (present work) with ages from 56 to 40 Ma (Figure 11). The U-Pb age of $56.4 +0.50/-0.70$ Ma (Figure 12, Tables 3 and 9) was obtained from sample *Gm-26* from a rhyolite north of Nuevo Ideal (Table 3). The available data allows us to establish that this volcanic event has not been synchronous in the entire region, and that there was a *hiatus* in the volcanic activity after 56 Ma in Nuevo Ideal, after 51 Ma in Santiago Papasquiaro and Durango, whereas in Nazas the *hiatus* began after 40 Ma (Figure 11). It's important to notice the presence of a population of 90-80 Ma zircons in rhyolite sample *Gm-26* from the Nuevo Ideal region, 40 km southeast of Santiago Papasquiaro (Figure 12, Tables 3 and 9). Those zircons indicate that the rhyolite has incorporated zircons from Cretaceous granitic or volcanic rocks that must underlie the area. An example of this is an 87 ± 1.8 Ma (K-Ar, hornblende) diorite pluton reported by Aguirre-Díaz and McDowell (1991) in the Nazas-Rodeo region, ~90 km northeast of Nuevo Ideal.

The late Eocene-early Oligocene volcanic episode began *ca.* 38 Ma and is composed of acid to intermediate rocks (Figure 11). In Santiago Papasquiaro the volcanism continued into the early Oligocene. In the Nuevo Ideal region the age of the Coneto Rhyolite, the youngest unit of this volcanic sequence, is unknown. Volcanic activity is reported from 31 Ma to *ca.* 28 Ma in Durango and from 34 to 29 Ma near Nazas (Figure 11).

Volcanic activity ceased in late Oligocene time, and continental epiclastics were deposited in topographic depressions. During Neogene and Quaternary time, non-consolidated clay, sand and conglomerate were deposited. In the Miocene, basalt flows with ages ~24 Ma were emplaced in the Nazas region (Luhr *et al.*, 2001), whereas in Santiago

Papasquiaro and Durango basalts are younger, with ages from 10 to 12 Ma (Figure 11). The Durango Volcanic Field in Nuevo Ideal and Durango is composed of several volcanoes and basalt flows of Quaternary age (Albritton, 1958) (Figures 1, 2 and 11).

Extensional deformation (D1) initiated during the emplacement of the late Eocene-early Oligocene volcanic rocks. The coeval faulting and volcanism is inferred because the lower stratigraphic units show slightly greater tilts. D1 generated NW striking faults of the SLTFS in the north of the study area and NNW striking faults of the Santiago Papasquiaro half-graben in the south of the study area, creating an elongated depression where the Santiago formation was deposited. Some of the faults active during D1 were buried during deposition of the Santiago formation. We propose that RCOG began during D1 with the Santiago Papasquiaro half-graben and propagated southwards. This inference is based on the following observations: (a) vertical displacements of the RCOG diminish towards the south, from ~600 m near Santiago Papasquiaro to ~300 m near Otinapa, and the graben terminates 25 km south of Otinapa (Aranda-Gómez *et al.*, 1997; Henry and Aranda-Gómez, 2000); (b) the basin fill erosion is more advanced in the Santiago Papasquiaro half-graben than in the southernmost regions, near Otinapa and Rio Chico, where the erosion is incipient; (c) sedimentary deposits that fill the northern depressions are more than 300 m thick and thin southward to tens of meters (Aranda-Gómez *et al.*, 1997; Henry and Aranda-Gómez, 2000); (d) the basin system slopes northward, going gradually from average heights of 2100 masl in the south to 1700 masl in the north. We interpret that D1 initiated synchronously with the final stage of late Eocene-early Oligocene volcanism because, even though the collected data are scarce, the average tilting of El Cazadero andante and Puente Negro ignimbrite is ~17° SW, whereas the Balín ignimbrite average tilting is ~12° SW, forming a slight angular unconformity that could be observed in the

Table 8. LA-ICP-MS zircon data from sample *Pas-wb* of Balín ignimbrite

Spot number	U (ppm)	Th (ppm)	Th/U	$^{207}\text{Pb}/^{206}\text{Pb}$	$\pm 1\sigma$	$^{207}\text{Pb}/^{235}\text{U}$	$\pm 1\sigma$	$^{206}\text{Pb}/^{238}\text{U}$	$\pm 1\sigma$	$^{208}\text{Pb}/^{232}\text{Th}$	$\pm 1\sigma$	Rho	CORRECTED RATIOS				CORRECTED AGES (Ma)					
													$^{206}\text{Pb}/^{238}\text{U} \pm 1\sigma$	$^{207}\text{Pb}/^{235}\text{U} \pm 1\sigma$	$^{207}\text{Pb}/^{238}\text{U} \pm 1\sigma$	$^{208}\text{Pb}/^{232}\text{Th} \pm 1\sigma$						
40	1347	1644	1.12	0.04696	0.00122	0.03113	0.00091	0.00482	0.00006	0.00141	0.00002	0.46	31	0.4	31.1	0.9	47	54	28.5	0.4	31	0
45	802	441	0.51	0.0478	0.00315	0.03208	0.00234	0.00487	0.00008	0.00155	0.00007	0.33	31.3	0.5	32	2	89	137	31	1	31	1
24	1157	691	0.55	0.05596	0.00282	0.03832	0.00219	0.00497	0.00007	0.00155	0.00002	0.42	31.9	0.5	38	2	451	109	31.2	0.4	32	1
44	805	767	0.88	0.05343	0.0016	0.03642	0.00121	0.00498	0.00007	0.00155	0.00003	0.43	32	0.4	36	1	347	65	31.3	0.6	32	0
51	496	363	0.67	0.05715	0.00358	0.0392	0.00276	0.00497	0.00008	0.00155	0.00002	0.34	32	0.5	39	3	498	133	31.2	0.4	32	1
34	287	214	0.69	0.05689	0.00354	0.03915	0.00274	0.00499	0.00008	0.00155	0.00002	0.26	32.1	0.5	39	3	487	129	31.3	0.4	32	1
10	415	214	0.47	0.05678	0.00417	0.0396	0.00316	0.00506	0.00007	0.00157	0.00002	0.32	32.5	0.5	39	3	483	157	31.8	0.5	33	1
8	452	277	0.56	0.0522	0.00219	0.0363	0.00161	0.00507	0.00007	0.00163	0.00004	0.32	32.6	0.4	36	2	294	93	32.9	0.8	33	0
46	585	313	0.49	0.05356	0.00187	0.03774	0.0014	0.0051	0.00006	0.00175	0.00013	0.34	32.8	0.4	38	1	353	76	35	3	33	0
41	638	313	0.45	0.05704	0.0033	0.04019	0.00259	0.00511	0.00007	0.00159	0.00002	0.38	32.9	0.5	40	3	493	123	32.1	0.5	33	1
17	650	390	0.55	0.05543	0.00183	0.03912	0.00137	0.00511	0.00006	0.00162	0.00004	0.33	32.9	0.4	39	1	430	69	32.7	0.8	33	0
22	629	258	0.38	0.05037	0.00171	0.03537	0.0013	0.00514	0.00007	0.00166	0.00004	0.38	33	0.4	35	1	212	77	33.5	0.8	33	0
20	727	490	0.62	0.05466	0.00275	0.03884	0.00221	0.00515	0.00007	0.00161	0.00002	0.35	33.1	0.5	39	2	398	110	32.5	0.4	33	1
9	632	265	0.39	0.04774	0.00153	0.03388	0.00115	0.00515	0.00006	0.00148	0.00004	0.33	33.1	0.4	34	1	86	67	29.9	0.8	33	0
48	502	244	0.45	0.04987	0.00185	0.03517	0.00137	0.00515	0.00006	0.00166	0.00004	0.31	33.1	0.4	35	1	189	82	33.5	0.8	33	0
53	480	243	0.46	0.05357	0.00297	0.03801	0.00231	0.00515	0.00007	0.00161	0.00002	0.35	33.1	0.5	38	2	353	118	32.5	0.4	33	1
39	441	218	0.46	0.0523	0.0039	0.0372	0.00298	0.00516	0.00007	0.00162	0.00003	0.23	33.2	0.5	37	3	299	157	32.7	0.7	33	1
36	409	258	0.58	0.05726	0.00445	0.04112	0.00356	0.0521	0.00009	0.00162	0.00003	0.34	33.5	0.6	41	3	502	162	32.7	0.5	34	1
38	219	138	0.58	0.05321	0.00369	0.03827	0.00306	0.0522	0.00011	0.00163	0.00003	0.31	33.5	0.7	38	3	338	146	33	0.6	34	1
42	462	329	0.65	0.05222	0.00568	0.03761	0.00437	0.0522	0.00009	0.00164	0.00006	0.29	33.6	0.6	37	4	295	235	33	1	34	1
23	583	366	0.58	0.06099	0.00356	0.0441	0.00284	0.0524	0.00007	0.00162	0.00002	0.39	33.7	0.5	44	3	639	122	32.6	0.5	34	1
47	264	161	0.56	0.05574	0.00245	0.03987	0.00187	0.0524	0.00008	0.00157	0.00005	0.35	33.7	0.5	40	2	442	94	32	1	34	1
50	368	207	0.52	0.0606	0.00294	0.04375	0.00246	0.0524	0.00008	0.00162	0.00002	0.34	33.7	0.5	43	2	625	101	32.6	0.5	34	1
18	337	211	0.58	0.06198	0.00868	0.04497	0.00666	0.0526	0.00011	0.00162	0.00004	0.29	33.8	0.7	45	6	673	292	32.7	0.8	34	1
15	650	295	0.42	0.05816	0.00508	0.04212	0.00391	0.0525	0.00008	0.00163	0.00003	0.31	33.8	0.5	42	4	536	180	32.9	0.6	34	1
11	592	266	0.41	0.05215	0.00151	0.03799	0.00119	0.00528	0.00006	0.00162	0.00004	0.38	33.9	0.4	38	1	292	62	32.7	0.8	34	0
35	192	112	0.54	0.05686	0.00301	0.04173	0.00231	0.00534	0.00009	0.00163	0.00005	0.29	34.3	0.6	42	2	486	110	33	1	34	1
12	421	248	0.54	0.05048	0.00257	0.03678	0.00194	0.00534	0.00007	0.00163	0.00003	0.26	34.3	0.4	37	2	217	109	32.9	0.6	34	0
33	229	121	0.49	0.05356	0.00336	0.04094	0.00284	0.00554	0.00008	0.00174	0.00003	0.26	35.6	0.5	41	3	353	133	35	0.5	36	1

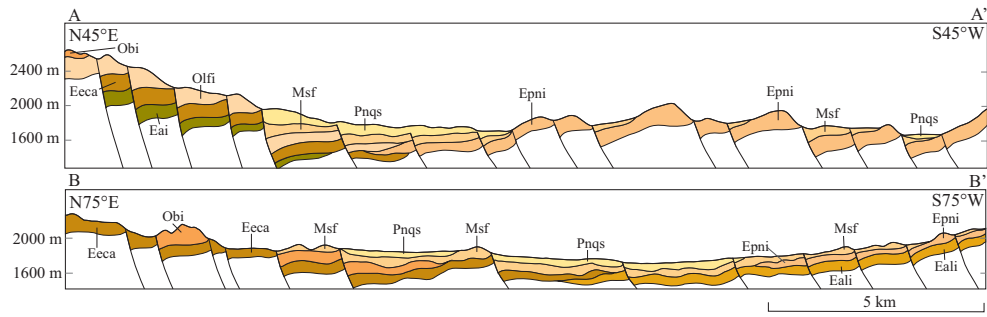


Figure 9. Cross sections of Santiago Papasquiaro valley in which the tilted block structure is observed. A-A' is a cross section of the SLTFS influence area, and B-B' is of the ORCG influence area. Unit names and color patterns as in Figure 4.

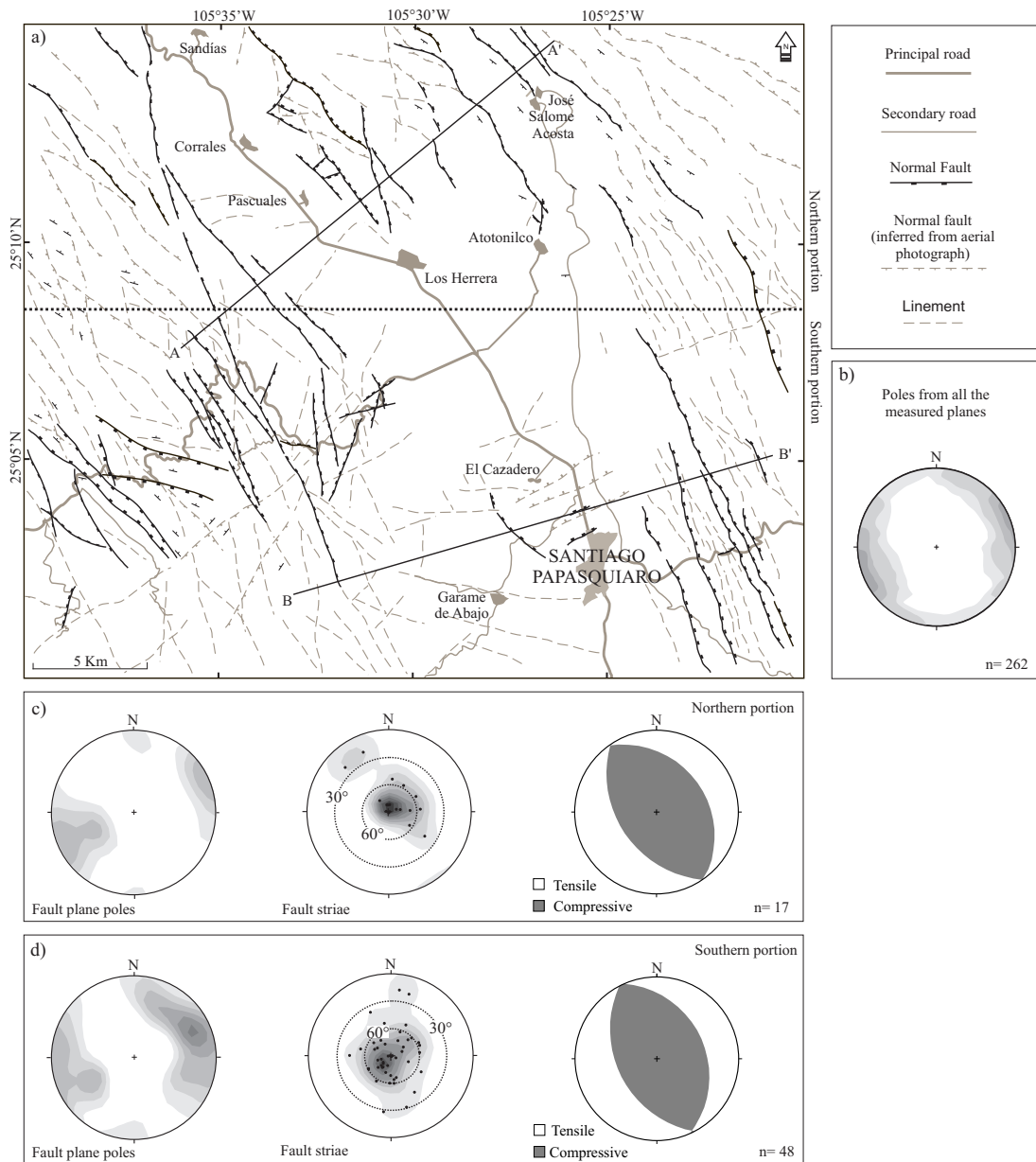


Figure 10. a: Map showing the principal structures in the studied area. b: Contour diagram that show poles of planes measured in all the study area. c: Contour diagrams of poles of fault planes, fault striae and deformation tensors presented as "beach ball" Diagrams, measured in the northern portion of the study area. d: Contour diagrams of poles of fault planes, fault striae and deformation tensors presented as "beach ball" Diagrams, measured in the southern portion of the study area. n: Data plotted in each diagram.

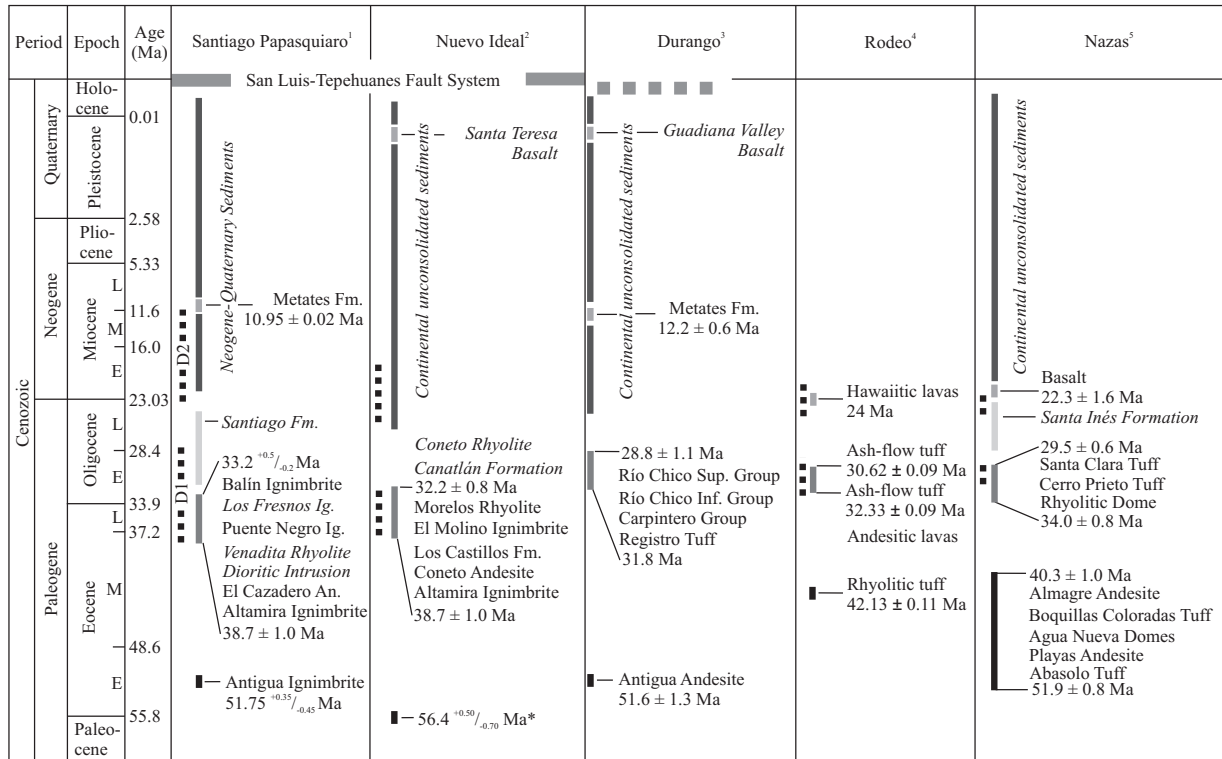


Figure 11. Regional lithostratigraphic correlation. ¹Lithostratigraphic column from this work. ²Nieto-Samaniego *et al.* (2012). ³McDowell and Keizer (1977). ⁴Lhur *et al.* (2001). ⁵Aguirre-Díaz and McDowell (1991). Dotted lines represent the main phases of extensional deformation. Two extensional deformation phases were recognized in Santiago Papasquiaro region (D1 and D2). *U-Pb age from rhyolite sample Gm-26.

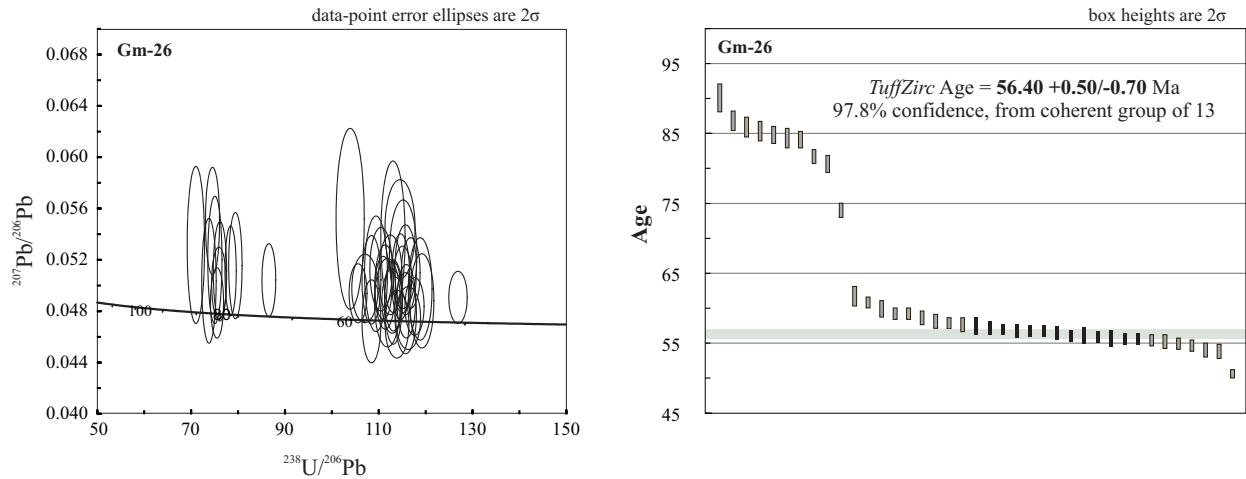


Figure 12. Zircon U-Pb data obtained by La-ICP-MS of sample *Gm-26* of the Nuevo Ideal region. a) Tera-Wasserburg diagram showing concordant data from rhyolite sample *Gm-26*. b) Mean weight age diagram for this sample.

transect across Santiago Papasquiaro-Los Altares highway.

In the early-middle Miocene time, after the deposition of Santiago formation, a second extensional deformation phase (D2) took place that reactivated NNW striking faults of the Santiago Papasquiaro half-graben. D2 was inferred from faults that cut and tilt the Santiago formation. Some of these faults can be observed on the Santiago Papasquiaro-

Garame de Abajo road and Santiago Papasquiaro-Nuevo Ideal highway. Some D2 faults were used later by feeder dikes of the equivalent Metates Formation; these dikes can be observed along the Santiago Papasquiaro-Nuevo Ideal highway and Santiago Papasquiaro-Francisco Javier Leyva road. Observed displacements on D2 NW faults of San Luis-Tepehuanes are less than 10 m; displacement in

Table 9. LA-ICP-MS U-Pb zircon data from sample GM-26 of Nuevo Ideal area.

Spot Number	U (ppm)	Th (ppm)	Th/U	CORRECTED RATIOS		CORRECTED AGES (Ma)																
				$^{207}\text{Pb}/^{235}\text{U}$	$\pm 1\sigma$	$^{207}\text{Pb}/^{238}\text{U}$	$\pm 1\sigma$	$^{208}\text{Pb}/^{232}\text{Th}$	$\pm 1\sigma$	Rho	$^{206}\text{Pb}/^{238}\text{U}$	$\pm 1\sigma$	$^{207}\text{Pb}/^{235}\text{U}$	$\pm 1\sigma$	$^{208}\text{Pb}/^{232}\text{Th}$	$\pm 1\sigma$						
58	2436	795	0.3	0.04907	0.00083	0.05335	0.00097	0.00788	0.00005	0.00272	0.00005	0.37	50.6	0.3	52.8	0.9	151	38	55	1	51	0.3
33	1087	536	0.46	0.0488	0.0015	0.05644	0.00196	0.08339	0.00007	0.00266	0.00002	0.32	53.8	0.5	56	2	138	71	53.6	0.5	54	0.5
44	839	341	0.38	0.04973	0.00163	0.0577	0.00208	0.0841	0.00007	0.00266	0.00002	0.29	54	0.5	57	2	183	75	53.6	0.5	54	0.5
53	2080	708	0.32	0.04837	0.00092	0.05653	0.00115	0.0835	0.00006	0.00285	0.00005	0.35	54.6	0.4	56	1	117	43	58	1	55	0.4
57	1105	507	0.42	0.05098	0.00112	0.06004	0.00139	0.0836	0.00006	0.00267	0.00005	0.32	54.9	0.4	59	1	240	49	54	1	55	0.4
20	1846	613	0.31	0.04746	0.001	0.05635	0.00129	0.086	0.00008	0.00279	0.00006	0.39	55.2	0.5	56	1	72	48	56	1	55	0.5
50	1199	463	0.36	0.04877	0.00117	0.05795	0.00144	0.0863	0.00006	0.00274	0.00006	0.26	55.4	0.4	57	1	137	54	55	1	55	0.4
21	1150	629	0.51	0.05122	0.00143	0.06107	0.00178	0.0864	0.00007	0.00266	0.00005	0.29	55.5	0.4	60	2	251	64	54	1	56	0.4
39	1017	317	0.29	0.04784	0.00129	0.05696	0.00161	0.0864	0.00007	0.00293	0.00006	0.3	55.5	0.4	56	2	91	61	59	1	56	0.4
45	773	395	0.47	0.05243	0.00173	0.06244	0.00215	0.0868	0.00009	0.0028	0.00005	0.29	55.7	0.6	61	2	304	75	57	1	56	0.6
28	1117	547	0.45	0.05047	0.00106	0.06047	0.00133	0.0869	0.00006	0.00275	0.00005	0.3	55.8	0.4	60	1	217	49	56	1	56	0.4
22	778	405	0.48	0.05438	0.00158	0.06547	0.00205	0.0873	0.00001	0.00283	0.00006	0.37	56	0.6	64	2	387	65	57	1	56	0.6
42	824	330	0.37	0.05067	0.00137	0.06048	0.00168	0.0872	0.00006	0.00278	0.00006	0.23	56	0.4	60	2	226	63	56	1	56	0.4
8	1353	863	0.59	0.04699	0.00108	0.05688	0.0014	0.0878	0.00008	0.00274	0.00005	0.36	56.4	0.5	56	1	49	50	55	1	56	0.5
32	1310	657	0.46	0.04922	0.00113	0.0599	0.00144	0.0884	0.00006	0.00286	0.00005	0.3	56.7	0.4	59	1	158	54	58	1	57	0.4
54	1007	429	0.39	0.04863	0.00131	0.05926	0.00165	0.0884	0.00006	0.00285	0.00007	0.25	56.7	0.4	58	2	130	60	58	1	57	0.4
27	484	150	0.29	0.05338	0.00241	0.06562	0.00309	0.0885	0.00008	0.00277	0.00003	0.21	56.8	0.5	65	3	362	102	55.9	0.6	57	0.5
30	1384	779	0.52	0.04878	0.00102	0.05955	0.00133	0.0886	0.00007	0.0028	0.00005	0.35	56.9	0.4	59	1	137	49	57	1	57	0.4
23	1139	579	0.47	0.05083	0.00127	0.06221	0.00165	0.0889	0.00008	0.00285	0.00006	0.34	57.1	0.5	61	2	233	58	58	1	57	0.5
11	991	480	0.45	0.04866	0.00141	0.0598	0.00183	0.0894	0.00009	0.0029	0.00006	0.32	57.4	0.6	59	2	131	67	59	1	57	0.6
15	1398	506	0.33	0.04988	0.00134	0.06175	0.00184	0.0898	0.00007	0.00283	0.00002	0.3	57.6	0.5	61	2	190	62	57.2	0.5	58	0.5
52	955	440	0.43	0.04982	0.001	0.06174	0.00131	0.0901	0.00006	0.00295	0.00006	0.32	57.8	0.4	61	1	187	45	60	1	58	0.4
46	678	335	0.46	0.05127	0.00133	0.06394	0.00175	0.0905	0.00008	0.00294	0.00006	0.32	58.1	0.5	63	2	253	60	59	1	58	0.5
12	740	269	0.34	0.05091	0.00184	0.06415	0.00253	0.09014	0.00008	0.00288	0.00003	0.29	58.6	0.5	63	2	237	84	58.1	0.5	59	0.5
16	1055	448	0.39	0.05044	0.00141	0.06396	0.00185	0.09022	0.00007	0.00284	0.00006	0.26	59.2	0.4	63	2	215	65	57	1	59	0.4
34	1383	751	0.5	0.04977	0.00109	0.06335	0.00156	0.09034	0.00001	0.00287	0.00007	0.46	59.9	0.6	62	1	184	51	58	1	60	0.6
51	1202	716	0.55	0.04939	0.00094	0.06435	0.00132	0.09047	0.00007	0.00303	0.00005	0.37	60.8	0.4	63	1	166	43	61	1	61	0.4
10	502	163	0.3	0.05519	0.00288	0.07323	0.00406	0.09062	0.00011	0.003	0.00004	0.24	61.7	0.7	72	4	420	118	60.6	0.8	62	0.7
14	1012	1178	1.08	0.05042	0.00116	0.07989	0.00192	0.09115	0.00008	0.00336	0.00006	0.29	74	0.5	78	2	214	53	72	1	74	0.5
56	641	274	0.4	0.05155	0.00169	0.08947	0.00318	0.09259	0.00009	0.00396	0.00003	0.26	80.6	0.6	87	3	266	73	79.8	0.6	81	0.6
47	594	238	0.37	0.05114	0.00143	0.08958	0.00258	0.09275	0.00008	0.00422	0.00014	0.24	81.7	0.5	87	2	247	64	85	3	82	0.5
9	556	276	0.46	0.0511	0.00158	0.09221	0.00295	0.09313	0.0001	0.00422	0.00008	0.26	84.1	0.6	90	3	245	71	85	2	84	0.6
17	701	418	0.55	0.05017	0.00115	0.09114	0.00223	0.09317	0.00011	0.00419	0.00008	0.35	84.3	0.7	89	2	203	53	85	2	84	0.7
35	588	258	0.41	0.04864	0.00112	0.08878	0.00215	0.09324	0.0001	0.00425	0.00009	0.31	84.8	0.6	86	2	131	54	86	2	85	0.6
38	359	159	0.41	0.05199	0.00203	0.09515	0.00338	0.09332	0.00011	0.00425	0.00013	0.21	85.3	0.7	92	4	285	90	86	3	85	0.7
40	382	214	0.52	0.05502	0.00171	0.10109	0.00324	0.09341	0.00011	0.00425	0.0001	0.24	85.9	0.7	98	3	413	70	86	2	86	0.7
36	400	124	0.29	0.0672	0.01546	0.11875	0.02736	0.09343	0.00019	0.00436	0.00012	0.05	86	1	114	25	844	503	88	2	86	+
18	411	183	0.41	0.05037	0.00199	0.09409	0.03937	0.09355	0.00012	0.00427	0.00004	0.22	86.8	0.7	91	4	212	91	86.2	0.8	87	0.7
41	278	117	0.39	0.05316	0.0025	0.1034	0.00499	0.09408	0.00015	0.00448	0.00016	0.22	90.1	1	100	5	336	107	97	3	90	1

this system might have migrated to the east-southeast to the Santiaguillo graben where the peak of deformation ended in early Miocene (Nieto-Samaniego *et al.*, 2012).

Minor extensional deformation (D3) in the Pliocene-Quaternary is evidenced from NE faults that affected the Neogene-Quaternary non-consolidated sediments. North of Santiago Papasquiaro two faults were measured in the recent basin fill deposits, with displacements of ~2 meters (Figure 13). Nieto-Samaniego *et al.* (2012) documented seismic activity in the Santiaguillo graben region. The reported seismicity supports that there is active deformation in the region, which could be responsible for the younger faults mapped in the study area.

6. Conclusions

The main conclusions from this study as well as the improvements in the knowledge of Cenozoic evolution of the northwestern Mesa Central of Mexico are:

- Six new U-Pb isotopic dates contribute to constraining the time of two volcanic pulses during the Cenozoic and the hiatus between them: The first volcanic pulse, referred to in the text as the Paleocene-middle Eocene volcanic pulse, is represented in the study area by 51.7 Ma rocks. The second volcanic pulse occurred in the late Eocene-early Oligocene and spanned from: 38.7 to 33.2 Ma.
- Three units with late Oligocene to Quaternary ages were distinguished in the study area: Santiago formation, basalts equivalent to the Metates Formation and non-consolidated sediments of the Neogene-Quaternary.
- Reported 56.4 and 51.7 Ma volcanic rocks confirm the existence of a pre-Oligocene volcanism pulse in the northwestern portion of the Mesa Central.
- Oligocene volcanism has been reported extensively



Figure 13. Photograph of NE striking faults that affect some of the Neogene-Quaternary unconsolidated deposits north of Santiago Papasquiaro.

in the Mesa Central. In the study area this volcanic pulse initiated at *ca.* 37-38 Ma, shortly earlier than in other areas, and lasted *ca.* 5 Ma. There is a hiatus between those two volcanic pulses, as has been previously reported in other areas of the Mesa Central (Nieto-Samaniego *et al.*, 2005; Loza-Aguirre *et al.*, 2008). The data presented here allows arguing that this hiatus lasted *ca.* 10 Ma in Santiago Papasquiaro.

- Three deformational phases were identified in the study area: D1 during the late Eocene-early Oligocene formed NW striking faults of the San Luis-Tepehuanes fault system and NNW striking faults of the Santiago Papasquiaro half-graben. The deformation migrated southward from Santiago Papasquiaro to the Rio Chico-Otinapa region. D2 during the early-middle Miocene reactivated NNW and faults NW. D3 during Pliocene-Quaternary formed minor displacement NE striking faults that cut unconsolidated deposits.
- Late Oligocene to Quaternary units record a new stage in the tectono-magmatic evolution of this region of the MC: the end of explosive acid volcanism of the SMOc, changing to an erosional phase with deposition of continental sediments in graben structures with small amounts of basaltic magmatism.

In the study area, crustal extension and volcanism occurred synchronously from late Eocene to present. The peak of extension and volcanism extended from late Eocene to early Oligocene.

Acknowledgements

The present work was financed by CONACYT projects 80142 and 049049. All the lab work was done at the Centro de Geociencias, Universidad Nacional Autónoma de México. We thank Juan Tomas Vázquez Ramírez for thin section preparation. Reviews by Fred McDowell and Christopher Henry substantially improved this manuscript.

References

- Aguirre-Díaz, G.J., McDowell, F.W., 1991, The volcanic section at Nazas, Durango, Mexico, and the possibility of widespread Eocene volcanism within the Sierra Madre Occidental: *Journal of Geophysical Research*, 96, 13373-13388.
 Aguirre-Díaz, G.J., McDowell, F.W., 1993, Nature and timing of faulting and synextensional magmatism in the southern Basin and Range, central-eastern Durango, Mexico: *Geological Society of America Bulletin*, 105, 1435-1444.
 Albritton, Jr., C.C., 1958, Quaternary Stratigraphy of the Guadiana Valley, Durango, Mexico: *Bulletin of the Geological Society of America*, 69, 1197-1216.
 Andersen T., 2002, Correction of common lead in U-Pb analysis that do not report ^{204}Pb : *Chemical Geology*, 192, 59-79.

- Aranda-García, M., Gómez-Luna, M.A., Contreras y Montero, B., 1987, El Jurásico Superior (Kimmeridgiano-Tithoniano) en el área de Santa María del Oro, Durango, México: Revista de la Sociedad Mexicana de Paleontología, 1, 75-87.
- Aranda-Gómez, J.J., Henry, C.D., Luhr, J.F. and McDowell, F.W., 1997, Cenozoic volcanism and tectonics in NW Mexico a transect across the Sierra Madre Occidental volcanic field and observations on extension related magmatism in the southern Basin and Range and Gulf of California tectonic provinces, in Aguirre-Díaz, G.J., Aranda-Gómez, J.J., Carrasco-Núñez, G. and Ferrari, L. (eds.), Magmatism and tectonics in the central and northwestern Mexico a selection of the 1997 IAFCM general Assembly excursions: México D.F., México, Universidad Nacional Autónoma de México, Instituto de Geología, 41-84.
- Araujo-Mendieta, J., Arenas-Partida, R., 1986, Estudio Tectónico-Sedimentario en el Mar Mexicano, Estados de Chihuahua y Durango: Boletín Sociedad Geológica Mexicana, 47, 43-71.
- Contreras-Montero, B., Martínez-Cortes, A., Gómez-Luna, M.E., 1988, Bioestratigrafía y Sedimentología del Jurásico Superior en San Pedro del Gallo, Durango, México: Revista del Instituto Mexicano del Petróleo, 20, 5-49.
- Córdoba, D.A., 1963, Geología de la región entre Río Chico y Llano Grande, Municipio de Durango, Estado de Durango, in Cséna, Z. (ed.), Estudios geológicos en los Estados de Durango y San Luis Potosí: México, D.F., México, Universidad Nacional Autónoma de México, Instituto de Geología, 71, 1-21.
- Córdoba, D.A., 1988, Estratigrafía de las rocas volcánicas de la región entre Sierra de Gamón y Laguna de Santiaguillo, Estado de Durango: Revista del Instituto de Geología, Universidad Nacional Autónoma de México, 7, 136-147.
- Ferrari, L., Valencia-Moreno, M., Bryan, S., 2005, Magmatismo y tectónica en la Sierra Madre Occidental y su relación con la evolución de la margen occidental de Norteamérica: Boletín de la Sociedad Geológica Mexicana, 57, 343-378.
- Henry, C.D., Aranda-Gómez, J.J., 2000, Plate interactions control middle-late Miocene, proto-Gulf and Basin and Range extension in the southern Basin and Range: Tectonophysics, 318, 1-26.
- Instituto Nacional de Estadística Geografía e Informática (INEGI), 1990, Carta Hidrológica de Aguas Subterráneas, Santiago Papasquiaro, G13-8, Esc. 1:250000: México, D.F., México, Secretaría de Programación y Presupuesto, Instituto Nacional de Estadística, Geografía e Informática, 1 mapa.
- Instituto Nacional de Estadística Geografía e Informática (INEGI), 2000, Carta Topográfica, Santiago Papasquiaro, G13C48, Esc. 1:50000: México, D.F., México, Secretaría de Programación y Presupuesto, Instituto Nacional de Estadística, Geografía e Informática, 1 mapa.
- Iriondo, A., Kunk, M.J., Winick, J.A., CRM, 2003, $^{40}\text{Ar}/^{39}\text{Ar}$ Dating Studies of Minerals and Rocks in various areas in Mexico: USGS/CRM Scientific Collaboration (Part I): Denver, Colorado, USGS 2004, disponible en <http://pubs.usgs.gov/of/2003/ofr-03-020/OFR-03-020-508eng.pdf>
- Iriondo, A., Kunk, M.J., Winick, J.A., CRM, 2004, $^{40}\text{Ar}/^{39}\text{Ar}$ Dating Studies of Minerals and Rocks in various areas in Mexico: USGS/CRM Scientific Collaboration (Part II): Denver, Colorado, USGS 2004, http://pubs.usgs.gov/of/2004/1444/OF2004_1444_508.pdf
- Loza-Aguirre, I., Nieto-Samaniego, A.F., Alaniz-Álvarez, S.A., Iriondo, A., 2008, Relaciones estratigráfico-estructurales en la intersección del sistema de fallas San Luis-Tepehuanes y el graben de Aguascalientes, México central, Revista Mexicana de Ciencias Geológicas, 25(3), 533-548.
- Ludwig K.R., 2008, Isoplot 3.7. A geochronological toolkit for Microsoft Excel: Berkeley, California, USA, Berkeley Geochronology Center Special Publication, No. 4, 77pp, disponible en <http://www.bgc.org/isoplot/etc/isoplot/>
- Luévano-Pinedo, J.A., Millán-Quezada, L., Guereca-Meza, R., 2003, Carta Geológico-Minera Santiago Papasquiaro G13-C48, escala 1:50000: Pachuca, Hidalgo, Consejo de Recursos Minerales, 1 hoja con texto explicativo.
- Luhr, J.F., Henry, C.D., Housh, T.B., Aranda-Gómez, J.J., McIntosh, W.C., 2001, Early extension and associated mafic alkalic volcanism from the southern Basin and Range Province: Geology and petrology of the Rodeo and Nazas volcanic fields, Durango, México: Geological Society of America Bulletin, 113, 760-773.
- McDowell, F.W., Keizer, R.P., 1977, Timing of mid-Tertiary volcanism in the Sierra Madre Occidental between Durango City and Mazatlán, Mexico: Geological Society of America Bulletin, 88, 1479-1487.
- McDowell, F.W., Clabaugh, S.E., 1981, The igneous history of the Sierra Madre Occidental and its relation to the tectonic evolution of western Mexico: Revista Instituto de Geología, Universidad Nacional Autónoma de México, 5, 195-205.
- Munguía-Rojas, P., García-Padilla, J.L., Armenta-Román, R., Cruz-Pérez, R., Camacho, J.M., De Santiago-Céspedes, J., 1998, Carta Geológico-Minera, Durango G13-11, escala 1:250000, Pachuca, Hidalgo, Consejo de Recursos Minerales, 1 hoja con texto explicativo.
- Munguía-Rojas, P., García-Padilla, J.L., Armenta-Román, R., Camacho, J.M., 2000, Carta Geológico-Minera, Santiago Papasquiaro G13-8, escala 1:250000: Pachuca, Hidalgo, Consejo de Recursos Minerales, 1 hoja con texto explicativo.
- Nieto-Samaniego, A.F., Alaniz Alvarez, S.A., Camprubí, A., 2005, La Mesa Central de México: estratigrafía, estructura y evolución tectónica cenozoica: Boletín de la Sociedad Geológica Mexicana, 57, 285-317.
- Nieto-Samaniego, A.F., Barajas-Gea, C.I., Gómez-González, J.M., Rojas, A., Alaniz-Alvarez, S.A., Xu, S.-S., 2012, Geología, evolución estructural (Eoceno al actual) y eventos sísmicos del Graben de Santiaguillo, Durango, México: Revista Mexicana de Ciencias Geológicas, 29, 115-130.
- Servicio Geológico Mexicano (SGM), 2007, Carta Geológica de la República Mexicana, escala 1:2000000, Pachuca, Hidalgo, Servicio Geológico Mexicano, 1 mapa.
- Solari, L.A., Gómez-Tuena, A., Bernal, J.P., Pérez-Arvizu, O., Tanner, M., 2010, U-Pb zircon geochronology by an integrated LA-ICP-MS microanalytical workstation: achievements in precision and accuracy: Geostandards and Geoanalytical Research, 34, 5-18.
- Solari, L.A., and Tanner M., 2011, UPb.age, a fast reduction script for LA-ICP-MS U-Pb geochronology: Revista Mexicana de Ciencias Geológicas, 28, 83-91.
- Solé, J., Salinas, J.C., González-Torres, E., Cendejas Cruz, J.E., 2007, Edades K/Ar de 54 rocas ígneas y metamórficas del occidente, centro y sur de México: Revista Mexicana de Ciencias Geológicas, 24, 104-119.
- Swanson, E.R., Keizer, R.P., Lyons, J.I., Clabaugh, S.E., 1978, Tertiary volcanism and caldera development near Durango City, Sierra Madre Occidental, Mexico: Geological Society of America Bulletin, 89, 1000-1012.
- Zaldívar, R.J., Garduño, M.V.H., 1984, Estudio estratigráfico y estructural de las rocas del Paleozoico Superior de Santa María del Oro, Durango y sus implicaciones tectónicas: Sociedad Geológica Mexicana, Memorias 7^a Convención Nacional, 28-39.

Manuscript received: April 4, 2012.

Corrected manuscript received: June 7, 2012.

Manuscript accepted: June 6, 2012.